Nanotechnology, Science and Applications

Dovepress

open access to scientific and medical research

Open Access Full Text Article

ORIGINAL RESEARCH

Lipid Nanosystems and Serum Protein as Biomimetic Interfaces: Predicting the Biodistribution of a Caffeic Acid-Based Antioxidant

This article was published in the following Dove Press journal:
Nanotechnology, Science and Applications

Eduarda Fernandes [1,2]
Sofia Benfeito [3]
Fernando Cagide [3]
Hugo Gonçalves [4]
Sigrid Bernstorff [5]
Jana B Nieder [2]
M Elisabete CD Real Oliveira [1]
Fernanda Borges [3]
Marlene Lúcio [1,6]

[1]Departamento de Física da Universidade do Minho, CF-UM-UP, Centro de Física das Universidades do Minho e Porto, Campus de Gualtar, Braga, 4710-057, Portugal; [2] Ultrafast Bio- and Nanophotonics Group, INL – International Iberian Nanotechnology Laboratory, Braga, Portugal; [3]CIQUP/Department of Chemistry and Biochemistry, Faculty of Sciences, University of Porto, Porto, Portugal; [4]Paralab, SA, Valbom, 4420-392, Portugal; [5]Elettra-Sincrotrone Trieste S. C.p.A.,, Basovizza, Trieste, I-34149, Italy; [6]CBMA, Centro de Biologia Molecular e Ambiental, Departamento de Biologia, Universidade do Minho, Campus de Gualtar, Braga 4710-057, Portugal

Correspondence: Marlene Lúcio
Universidade do Minho, Campus de Gualtar, Braga 4710-057, Portugal
Email mlucio@fisica.uminho.pt

Fernanda Borges
CIQUP/Department of Chemistry and Biochemistry, Faculty of Sciences, University of Porto, Porto, Portugal
Email fborges@fc.up.pt

Purpose: $AntiOxCIN_3$ is a novel mitochondriotropic antioxidant developed to minimize the effects of oxidative stress on neurodegenerative diseases. Prior to an investment in pre-clinical in vivo studies, it is important to apply in silico and biophysical cell-free in vitro studies to predict $AntiOxCIN_3$ biodistribution profile, respecting the need to preserve animal health in accordance with the EU principles (Directive 2010/63/EU). Accordingly, we propose an innovative toolbox of biophysical studies and mimetic models of biological interfaces, such as nanosystems with different compositions mimicking distinct membrane barriers and human serum albumin (HSA).

Methods: Intestinal and cell membrane permeation of $AntiOxCIN_3$ was predicted using derivative spectrophotometry. $AntiOxCIN_3$ –HSA binding was evaluated by intrinsic fluorescence quenching, synchronous fluorescence, and dynamic/electrophoretic light scattering. Steady-state and time-resolved fluorescence quenching was used to predict $AntiOxCIN_3$-membrane orientation. Fluorescence anisotropy, synchrotron small- and wide-angle X-ray scattering were used to predict lipid membrane biophysical impairment caused by $AntiOxCIN_3$ distribution.

Results and Discussion: We found that $AntiOxCIN_3$ has the potential to permeate the gastrointestinal tract. However, its biodistribution and elimination from the body might be affected by its affinity to HSA (>90%) and by its steady-state volume of distribution (VD_{SS}=1.89 ± 0.48 $L{\cdot}Kg^{-1}$). $AntiOxCIN_3$ is expected to locate parallel to the membrane phospholipids, causing a bilayer stiffness effect. $AntiOxCIN_3$ is also predicted to permeate through blood-brain barrier and reach its therapeutic target – the brain.

Conclusion: Drug interactions with biological interfaces may be evaluated using membrane model systems and serum proteins. This knowledge is important for the characterization of drug partitioning, positioning and orientation of drugs in membranes, their effect on membrane biophysical properties and the study of serum protein binding. The analysis of these interactions makes it possible to collect valuable knowledge on the transport, distribution, accumulation and, eventually, therapeutic impact of drugs which may aid the drug development process.

Keywords: biomimetic models, biophysical profiling, drug–membrane interaction, blood–brain barrier permeability, drug distribution, small and wide-angle X-ray diffraction

Introduction

Research over the past few decades has revealed the involvement of oxidative stress in several disease states, in particular those presenting an increased incidence with age, including cardiovascular events, cancer, diabetes mellitus and neurodegenerative

diseases.[1,2] The concept of an imbalance between oxidants and antioxidants has evolved in recent years embracing all the biological responses involving the disruption of redox signaling pathways. In normal circumstances, cells attempt to counteract the oxidant effects and restore the redox balance through a diversity of processes, namely the activation or silencing of genes encoding defensive enzymes and structural proteins.[3] However, an overproduction of reactive species (RS) resultant from oxidation can damage the integrity of various biomolecules, such as lipids, proteins, and DNA/RNA, leading to cell death.[4,5] The use of antioxidants capable to prevent and/or minimize RS levels inside the cell is considered a therapeutic solution to slow-down the progression of the radical cascade reactions. Notwithstanding, the problems found with bioavailability and druggability of antioxidants, among others, limit their success in clinical trials. This limitation is related mainly to biodistribution issues and to the fact that frequently antioxidants do not reach relevant sites of free radical generation. So, the development of new effective treatments for neurodegenerative diseases is still a challenge due to the restrictive passage across biological membranes, namely the blood brain barrier (BBB) in order to reach the Central Nervous System (CNS).[6]

The covalent link of a lipophilic cation, namely alkyl triphenylphosphonium (TPP), to an antioxidant has been proposed as an effective strategy to deliver this type of compounds specifically to mitochondria, the main source of RS that are generated as by-products of the electron transport chain.[7–9] In this context, a rational drug discovery program based on a dietary antioxidant (caffeic acid, Figure 1A) was accomplished by our group, giving rise to the first mitochondriotropic antioxidants, commonly named AntiOxCINs, based on a phenolic acid.[10] The results obtained so far indicated that AntiOxCIN$_3$ (Figure 1B) is a potent antioxidant able of mitochondrial accumulation and devoid of mitochondrial toxicity.[10]

Interestingly, TPP lipophilic cations have been described as an exception to the "rule of five" that is often used as preliminary predictor of relevant drug-like properties such as solubility, bioavailability, and ability to pass through phospholipid bilayers.[11,12] This exception is due to the unusual properties of being both relatively water soluble and membrane permeant, even with a rather large molar mass and partition coefficient, an indicator of high lipophilicity.[13] Among the mitochondriotropic compounds, it was found that the most lipophilic ones, till a limit on the number of methylene groups in the linker, presented the highest antioxidant potency.[14] In fact, it is consensual that lipophilicity is the major determinant in drugs' biodistribution, since it is intimately related to membrane permeability, which dictates the drug ability to pass through the different biological interfaces.[15] Otherwise, increasing lipophilicity leads to a reduction in aqueous solubility and in turn, to biodistribution due to the drug's high affinity to plasma proteins. Moreover, highly lipophilic drugs present usually poor oral absorption and are more vulnerable to CYP450 metabolism, and in consequence to a high hepatic clearance.

Considering the therapeutic interest of AntiOxCINs and assuming the oral administration of drugs as the most conventional route either by patient's choice or due to industrial reasons,[16] the oral administration of AntiOxCIN$_3$ was hypothesized. Although oral absorption is the most popular and convenient route, it is limited by drug physicochemical properties (low aqueous solubility and/or low membrane permeability), among other factors.[17] Upon oral administration of AntiOxCIN$_3$, the drug is expected to interact promptly with a number of biological interfaces that will constitute barriers to its biodistribution.[18,19] For orally

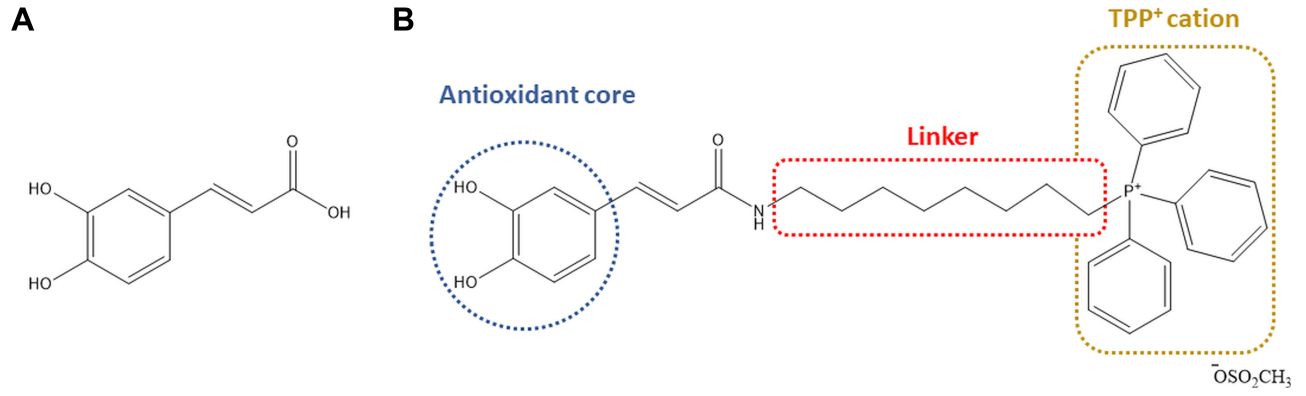

Figure 1 Chemical structures of caffeic acid (**A**) and mitochondriotropic antioxidant AntiOxCIN$_3$ (**B**).

administrated drugs, gastrointestinal (GI) absorption is the first physical barrier. The drug must be able to permeate through the intestinal epithelial barrier to guarantee bioavailability and biodistribution. After GI absorption, the drug will be exposed to plasma proteins in the bloodstream, the main function of which is to transport exogenous molecules through the body. However, the drug-plasma protein interaction must be reversible and balanced, since a too low or too high affinity will lead to biodistribution issues. When distributed to the body, drugs will continue to interact in a reciprocal way with other biological interfaces until they reach the therapeutic target. Also, even when the drug reaches the therapeutic target, its interaction with cell membranes can affect the rate of membrane partitioning and the subsequent penetration of the drug into the cytoplasm.[18] Hence, the partitioning in cell membranes and the drug/membrane interactions should be studied and characterized.[18,19]

Until today, the emergence of several biomimetic model membranes based on lipid nanosystems and biophysical techniques to study and characterize drug–membrane interactions have resulted in new concerns about how a drug influences membrane properties and vice-versa.[19–30] In our previous works, as well as in other studies, it is reported the correlations between the biological action and cytotoxicity of drugs and their biophysical effects in biomimetic membranes, eg by altering lipid membrane packing, decreasing lipid membrane transition temperatures or disturbing cooperativity of lipid unit cells, with consequent membrane biophysical impairment.[21,26–28,31,32] Additionally, several interesting reports[19,20,33–37] highlighted the importance of biomimetic models based on lipid nanosystems (liposomes, monolayers and supported lipid bilayers) to acquire molecular and functional information. The aim is using this acquired information to support the development of new drugs with better selectivity and reduced side effects[34]. This information can also assist to the design of new chemical entities with improved efficacy and reduced toxicity,[19,34,37] or even to understand the interaction of drug delivery nanosystems with biomembranes.[30,34,38,39]

Therefore, in this study, the interaction of AntiOxCIN$_3$ with the most relevant biointerfaces was studied and characterized allying in silico descriptors with different in vitro biophysical methods and biomimetic model systems to predict its biodistribution behavior. In order to mimic the journey of AntiOxCIN$_3$ in the body after oral administration, four different biomimetic interface models were considered: (i) micelles of intestinal biliary salts; (ii) human serum albumin (HSA); (iii) lipid nanosystems (lipid vesicles and lipid bilayers) used as membrane models, which are composed by phosphatidylcholine (PC) as the main phospholipid component of cell membranes; and (iv) lipid nanosystems (lipid vesicles) composed of lipids from the endothelial membrane of BBB mimicking this important lipid biointerface. Furthermore, several features of drug/biointerfaces' interaction were correlated with possible in vivo biodistribution issues of AntiOxCIN$_3$, giving some outputs of the chemical modifications needed to improve its performance. Thus, biomimetic membrane model systems were used to determine: (i) membrane distribution (K_d) in biomimetic models representative of membranes found in target and off-target tissues, (ii) drug location at membrane level, (iii) plasma protein binding (*PPB*) to infer the biodistribution of AntiOxCIN$_3$ and (iv) membrane biophysical characterization to predict possible toxic effects—at membrane level.

In summary, AntiOxCIN$_3$ is a potential drug candidate with application as antioxidant for the prevention/minimization of oxidative stress ascribed to neurodegenerative diseases, for which an oral administration is envisioned. Given the therapeutic potential of AntiOxCIN$_3$[10] and since there are no reports in the literature concerning the interaction of mitochondriotropic antioxidants with biomimetic interfaces, we propose the use of a membrane modelling biophysical approach to evaluate AntiOxCIN$_3$/biointerface interactions before progressing to the in vivo studies. This study of AntiOxCIN$_3$/biointerface interactions is a valuable step in assessing the biodistribution profile of this type of antioxidants.

Materials and Methods

Synthesis of AntiOxCIN$_3$

The synthetic strategy and general procedures used to obtain the mitochondriotropic antioxidant AntiOxCIN$_3$ have been previously described in Teixeira et al.[10]

Materials

The lipids 1,2-dimyristoyl-sn-glycero-3-phosphocholine (DMPC), 1.2-dipalmitoyl-sn-glycero-3-phosphocholine (DPPC) and the brain polar lipids (BPL) were obtained from Avanti Polar Lipids Inc. (INstruchemie, Delfzijl, Netherlands). The HSA and sodium deoxycholate (NaDC) were purchased from Sigma-Aldrich (Barcelona, Spain) at a purity grade of >99% and used without further purification. The fluorescent probes (±)-n-(9-anthroyloxy)

stearic acid (n=3, 6, 9 and 12, named as n-AS probes) and 1.6-diphenyl-1,3,5-hexatriene (DPH) were purchased from Invitrogen-Molecular Probes (Paisley, UK). All other chemicals were purchased either from Sigma-Aldrich or Cymit Quimica (Barcelona, Spain) and were of the highest commercially available purity. All aqueous solutions were prepared with ultrapure water produced by Millipore Milli-Q (resistivity = 18.2 MΩ·cm) or adjusted for pH with universal buffer solution.

In silico Prediction of Drug-Like Properties

Several molecular descriptors relevant to complement biophysical studies were calculated by in silico analysis using the module MarvinSketch® from ChemAxon® software (Budapest, Hungary): number of hydrogen bonds, polar (PSA) and van der Waals surface area (VWSA) and ionization state.

Preparation and Labelling of Lipid Nanosystems for Membrane Interactions

The membrane model systems were prepared by the lipid film hydration method followed by extrusion as previously reported.[40] Briefly, adequate portions of DMPC, DPPC or BPL were dissolved in chloroform, and subsequently evaporated to dryness under reduced pressure in a rotary evaporator (Buchi R210 Rotavapor, VWR International, Portugal). After hydration with ultrapure water, the suspension (1.00×10^{-3} M) was vortexed 20 min. The hydration was performed at a temperature above the main phase transition (T_m) of the lipid or lipid mixture (37 °C for DMPC and BPL; and 60 °C for DPPC). Lipid suspensions were then submitted to several freeze/thaw cycles and sequentially extruded through 400 nm, 200 nm and 100 nm nucleopore polycarbonate filters to produce large unilamellar vesicles (LUVs). LUVs are large unilamellar vesicles with a curvature closer to that of physiological membranes. As LUVs' preparation methods are easy and reproducible they are widely used as biomimetic systems to study the biophysical interactions between bioactives and membranes.[19,33,37,41,42] Besides lipid vesicles, micelles were also used as mimetic models of the biliary salt micelles and were prepared by aqueous dispersion of NaDC at a concentration above the critical micellar concentration (6 mM).[43]

In order to obtain labelled membrane nanosystems, ethanolic stock solutions of fluorescent probes were added to a chloroform solution of lipids in a lipid: probe molar ratio always greater than 100:1, to prevent structural changes of the membrane model system.[34] Lipid nanosystems were then prepared using a lipid film hydration method followed by extrusion as described above.

Derivative Spectrophotometry Studies to Evaluate Membrane Distribution of AntiOxCIN$_3$

The membrane distribution of AntiOxCIN$_3$ in NaDC ($K_{d(NaDC)}$), DMPC ($K_{d(PC)}$) and BPL ($K_{d(BBB)}$) was determined by using increasing concentrations of the lipid model systems (0–3.00×10^{-3} M for DMPC and BPL; 0–5.00×10^{-2} M for NaDC) and a fixed concentration of AntiOxCIN$_3$ (2.00×10^{-4} M), which were incubated for 30 minutes at 37 °C.

The absorption spectra (200–400 nm) were acquired (Perkin-Elmer Lambda 45 UV-VIS spectrophotometer) at 37.0 ± 0.1 °C for the NaDC and BPL membrane system and at 30, 33, 37, 40 and 45.0 ± 0.1 °C for the DMPC membrane model system. Derivative spectra were obtained from absorption spectra in accordance with the procedure previously published.[44] In the third derivative spectra, the spectral interferences promoted by the lipid suspensions were removed. K_d values were obtained by a non-linear regression from the graphical representation of λ_{max} or λ_{min} as a function of the concentration of lipid nanosystems ([MembraneModel] in mol·L^{-1}):

$$\frac{d^3A_T}{d\lambda^3} = \frac{d^3A_a}{d\lambda^3} + \frac{\left(\frac{d^3A_l}{d\lambda^3}\right)\cdot K_d\cdot[MembraneModel]\cdot V_l}{1+K_d\cdot[MembraneModel]\cdot V_l} \quad (1)$$

where A_T stands for the total absorbance of drug (in lipid and in aqueous media) and A_a and A_l are the absorbances in aqueous media and in lipid media, respectively. V_l refers to the lipid molar volume (L·mol^{-1}) and it is characteristic for each membrane model and can be calculated from the specific volumes of each lipid.[21,45]

Fluorescence Studies to Evaluate Interactions Between AntiOxCIN$_3$ and Membrane Model Systems

Steady-State and Lifetime Fluorescence Measurements

DMPC membrane model system was labelled with n-AS probes, wherein n represents a well-defined hydrocarbon chain position of a stearic acid (carbon 2, 6, 9 or 12) where the fluorophore (anthracene group) is attached. The

fluorescence of the fluorophore was monitored by lifetime and steady-state fluorescence studies to predict AntiOxCIN$_3$ location at membrane level. Increasing concentrations of AntiOxCIN$_3$ (0–3.0×10^{-2} M) and a fixed concentration of the labelled DMPC model system (5.0×10^{-2} M) were used. Steady-State fluorescence emission (Fluorolog-4 Spectrofluorometer, HORIBA Scientific) was obtained using $\lambda_{excitation}$=379 nm. Fluorescence excitation and emission spectra were recorded using slits of 2 and 6 nm, respectively, and an integration time of 1 s was used. Time-resolved fluorescence measurements (ISS Chronos BH equipped with a picosecond laser C10196, Hamamatsu) were performed at $\lambda_{excitation}$=379 nm, with a pulse duration of 80 ps, and set to a repetition rate of 10 MHz. A 435/40 nm BP filter (Brightline, Semrock) was placed in front of the photodetector (H7422P-40, Hamamatsu) whose signal was connected with the SYNC signal of the laser to the Time Correlated Single Photon Counting—TCSPC module (SPC130, Becker&Hickl). Fluorescence lifetimes were determined by fitting a bi-exponential decay model and using the ISS-VINCI analysis software. Both spectrometers were equipped with a temperature-controlled sample holder and measurements were made at 30, 37 and 45 °C to have additional data to distinguish the quenching mechanism.

The extent of fluorescence quenching induced by AntiOxCIN$_3$ in n-AS probes (n = 3, 6, 9 or 12) was evaluated by Stern–Volmer constant (K_{SV}) obtained by fitting data to the Stern–Volmer linear plots:

$$\frac{I_0}{I} or \frac{\tau_0}{\tau} = 1 - K_{SV} \cdot [AntiOxCIN_3]_M \quad (2)$$

where (I, τ) and (I_0, τ_0) are the steady-state fluorescence emission and lifetime of the probe, respectively, in the presence or in the absence of AntiOxCIN$_3$. [AntiOxCIN$_3$]$_M$ is the membrane concentration of AntiOxCIN$_3$ calculated as described elsewhere:[21]

$$[AntiOxCIN_3]_M = \frac{K_d \cdot [AntiOxCIN_3]_T}{K_d \cdot V_m + (1 - V_m)} \quad (3)$$

where K_d is the distribution coefficient of AntiOxCIN$_3$ in the membrane model system (calculated as described in Equation 1), [AntiOxCIN$_3$]$_T$ is the total concentration of AntiOxCIN$_3$ and V_m is the membrane volume fraction.

The efficacy of AntiOxCIN$_3$ to quench the fluorescence of each probe was evaluated by the bimolecular constant (K_q):[45]

$$K_q = \frac{K_{SV}}{\tau_0} \quad (4)$$

K_q is independent of intrinsic microenvironment changes sensed by each probe, which are reflected in the different values of τ_0 (measured by lifetime fluorescence studies) and was used to infer the relative location of AntiOxCIN$_3$ in the membrane model system. All fluorescence intensity data were corrected from absorption and inner filter effect.[45]

Fluorescence Anisotropy Measurements

The steady-state anisotropy, r_{SS}, of DPH probe (5.0×10^{-6} M) incorporated in DPPC model system (5.0×10^{-2} M), before and after AntiOxCIN$_3$ addition (2.0×10^{-2} M), was measured at 30.0 and 50.0 ± 0.1 °C (Fluorolog-4 Spectrofluorometer, HORIBA Scientific). These temperatures were chosen for the evaluation of the effect in the two lipid phases: gel phase, $L_{\beta'}$, present at temperatures below T_m (ie < 41 °C), and fluid phase, L_α, at temperatures above T_m (ie > 41 °C). The probe was excited with vertically polarized light at 325 nm and the emitted fluorescence intensities were recorded between 400 and 600 nm with an integration time of 0.5 s and automatic insertion of emission polarizer parallel (I_{VV}) or perpendicular (I_{VH}) to the excitation polarizer allowing the determination of r_{SS}:

$$r_{SS} = \frac{I_{VV} - G \cdot I_{VH}}{I_{VV} + 2 \cdot G \cdot I_{VH}} \quad (5)$$

where G is the ratio between I_{HV} and I_{HH} and it is the internal correction factor for the sensitivity of the spectrofluorometer for vertically (I_{HV}) and horizontally (I_{HH}) polarized light.

Steady-State and Synchronous Fluorescence Quenching for Plasma Protein Binding Evaluation

The fluorescence excitation and emission spectra of increasing AntiOxCIN$_3$ concentrations (0 to 3.5×10^{-4} M) with fixed HSA concentration (2.0×10^{-6} M) were acquired at 25.0, 30.0, 37.0, 40.0 and 45.0 ± 0.1 °C (Perkin-Elmer LS-50B), with $\lambda_{excitation}$ of 223 nm and $\lambda_{emission}$ of 342 nm, both with slits of 5 nm. The quenching of HSA fluorescence promoted by increasing concentrations of AntiOxCIN$_3$ can be described by the following binding isotherm equation:[45]

$$\%Quenching = \frac{y_{max} n_{HSA}}{1 + \frac{K_{diss}}{[AntiOxCIN_3]}} \quad (6)$$

in which y_{max} is the maximum fluorescence quenching recorded, n_{HSA} is the number of binding sites of HSA to

AntiOxCIN$_3$. K_{diss} is the dissociation constant from which it is possible to calculate the binding constant (K_{bind}):

$$K_{bind} = \frac{1}{K_{diss}} \quad (7)$$

The % of plasma protein binding (*PPB*) can be obtained from the in vitro values of K_{bind}:[46]

$$PPB = \frac{100}{1 + \frac{1}{C_P \cdot K_{bind}}} \quad (8)$$

where C_P is the physiological plasma protein concentration (750 μM).[46]

Furthermore, the next equation describes the relation between K_{bind} value and the Gibbs free energy (ΔG) of the binding complex by:

$$\Delta G_{bind} = -R \cdot T \cdot \ln K_{bind} \quad (9)$$

where R is the ideal gas constant and T is the temperature in Kelvin (K). This equation can also be written as the van't Hoff equation:

$$\ln K_{bind} = \frac{-\Delta H}{R \cdot T} + \frac{\Delta S}{R} \quad (10)$$

The synchronous fluorescence measurements were obtained by the simultaneous scan of the excitation and emission monochromators, taking 31 readings in the range of 200–500 nm with 5 nm of increment (Perkin Elmer LS50B). Characteristic $\Delta\lambda$ values for tyrosine (15 nm) and tryptophan (60 nm) residues were used.[47]

Synchrotron Small- and Wide-Angle X-Ray Scattering Studies

For X-ray scattering experiments, the membrane model systems (DPPC and BPL) in the presence or absence of AntiOxCIN$_3$ were transferred into X-ray transparent glass capillaries with 1.5 mm diameter (Hilgenberg, Malsfeld, Germany). Capillaries were sealed using a flame and stored at 4 °C. Small- and Wide-Angle X-ray Scattering (SAXS and WAXS) measurements were performed at the Austrian SAXS/WAXS beamline at the synchrotron light source ELETTRA (Trieste, Italy) employing monochromatic synchrotron radiation with wavelength of 1.54 Å and X-ray energy of 8 keV. WAXS and SAXS patterns were recorded using a2D Pilatus 100K and 2D Pilatus3 1M detector system, respectively, with a pixel size of 172 μm at positions that covered the typical diffraction spacing (s) range:

$$s = \frac{2 \cdot \sin\theta}{\lambda} \quad (11)$$

where λ is the wavelength and 2θ is the scattering angle of interest. The diffraction spacings (s) were calibrated using the lamellar peaks of silver behenate (SAXS) and *p*-bromo benzoic acid (WAXS) as standards. From the s values correspondent to the position of the first-order Bragg peak of each lipid phase, long distances (d_L in the case of SAXS) and short distances (d_S in the case of WAXS) were determined:

$$d_L \text{ or } d_s = \frac{1}{s} \quad (12)$$

The full width at half maximum (*fwhm*) of the Bragg peaks were used to calculate the correlation length between the lipid bilayers (ξ):

$$\xi = \frac{2 \cdot \pi}{fwhm} \quad (13)$$

Measurements were performed in the ranges 20–56 °C and 20–90 °C, for DPPC and BPL membrane systems, respectively, both thermostated with a water bath (stability ± 0.1 °C, Unistat CC, Huber, Offenburg, Germany) to obtain the diffraction patterns of typical lipid phases ($L_{\beta'}$, ripple phase $P_{\beta'}$ and L_α) and the effect of AntiOxCIN$_3$ in such phases was evaluated. The data acquired was analyzed as previously described in other reports.[21]

Dynamic and Electrophoretic Light Scattering Studies

The affinity of AntiOxCIN$_3$ to HSA was confirmed by Dynamic and Electrophoretic Light Scattering (DLS and ELS). The hydrodynamic radii (R_h) and zeta-potential of free and complexed HSA were measured at 25.0, 30.0, 37.0, 40.0 and 45.0 ± 0.1 °C to follow the HSA-AntiOxCIN$_3$ complexation.[48] For each sample, at least three measurements with 100 s of stabilization time were performed.

DLS technique was also used to evaluate the effect of AntiOxCIN$_3$ addition in the T_m and cooperativity (B) of the DPPC membrane model system.[21,48] Thus, the light scattered (Mean Count Rate, *MCR*) by membrane system (5.0×10^{-2} M) in the absence and in the presence of AntiOxCIN$_3$ (2.0×10^{-2} M) was monitored as function of temperature (T) between 30 and 55°C (with intervals of 1 °C and 2 min of equilibration time). The results were fitted with a sigmoidal function based on a modified Boltzmann equation:[21,48]

$$MCR = b_1 + m_1 \cdot T + \frac{b_2 - b_1 + m_2 \cdot T - m_1 \cdot T}{1 + 10^{B \cdot \left(\frac{1}{T} - \frac{1}{T_m}\right)}} \quad (14)$$

where m_1 and m_2 are the slopes resultant from the linear fitting to the data before and after T_m, respectively, and b_1 and b_2 are the corresponding y-intercepts.

All DLS and ELS studies were performed in Zetasizer Nano ZS (Malvern Panalytical, Paralab, Portugal), using disposable polystyrene cells with the addition of a dip cell (ZEN1002) when ELS studies were performed.

Modelling Biodistribution from in vitro Parameters

The $LogK_d$ value, which is dependent on the membrane model systems, can be used along with in silico descriptors to predict several biodistribution parameters using mathematical models. Thus, the value of $LogK_{d(PC)}$ was used to predict AntiOxCIN$_3$ bioaccumulation (represented by the bioaccumulation constant, $K_{bioaccumulation}$), which is related to tissue blood flow (Q) and its volume (V):[16]

$$K_{bioaccumulation} = \frac{Q}{V \cdot K_{d(PC)}} \quad (15)$$

As an assessment of whether the drug is accumulated in adipose tissue, the adipose store index (ASI) of AntiOxCIN$_3$ was calculated using the following equation:[49]

$$ASI = 1.81 \cdot LogK_{d(PC)} - LogK_{d(PC)} + 0.40 \quad (16)$$

Moreover, according to Waterbeem and Kansy,[50] the obtained distribution coefficient in the BPL model system – $LogK_{d(BBB)}$ – can be related to $LogBB$. $LogBB$ can be defined as the logarithm of the ratio of drug concentrations in brain and in blood and reflects the relative affinity differences of the drug between the plasma proteins and brain tissue:[51]

$$LogBB = 0.388 \cdot LogK_{d(BBB)} - 0.00618 \cdot V_l + 1.359 \quad (17)$$

where V_l is the molar volume of the membrane model system used calculated from the specific lipid volumes.[21,45]

Additionally, it is possible to calculate the BBB permeability-surface area product (PS, quantified as $LogPS$):[51]

$$LogPS = -2.19 + 0.262 \cdot LogK_{d(BBB)} + 0.0583 \cdot VWSA_B - 0.00897 \cdot PSA \quad (18)$$

where VWSA$_B$ is the van der Walls surface area of the basic atoms that indicates the basicity of a compound.

One of the most useful pharmacokinetic parameters to describe the biodistribution of a drug is the Steady-State Volume Distribution (VD_{SS}).[52] This predictor translates the influence of the PPB, permeability, partitioning and active transport in the physiological distribution of the drug.[52] The first physiological mathematical model of VD_{SS} for predicting the biodistribution of the neutral and basic drugs was proposed with basis on human clinical pharmacokinetic data of a large set of drugs (670 drugs):[53]

$$VD_{SS} = V_P\left(1 + R_{\frac{E}{I}}\right) + f_u \cdot V_P\left(\frac{V_E}{V_P} - R_{\frac{E}{I}}\right) + \frac{V_R \cdot f_u}{f_{ut}} \quad (19)$$

where V_P and V_E are the plasma and extracellular fluid volumes with corresponding value in human of 0.0436 and 0.0151 L·Kg^{-1}.[53] $R_{E/I}$ represents the ratio of extravascular and intravascular proteins, and is strictly referred to the distribution of albumin, assuming an approximate value of 1.4.[53] V_R is defined as the physical volume into which the drug distributes minus the extracellular space (0.380 L·Kg^{-1}).[53] f_u and f_{ut} are, respectively, the unbound drug fraction in plasma and the unbound fraction in tissues.[53]

The value of f_u can be obtained by:[46]

$$f_u = 1 - \frac{PPB}{100} \quad (20)$$

Finally, f_{ut} can be obtained by the equation proposed by Lombardo et al:[53]

$$Logf_{ut} = -0.0289 - 0.1739 \cdot LogK_{d(PC)} - 0.8324 \cdot f_{i(7.4)} + 1.0400 \cdot Logf_u \quad (21)$$

where $f_{i(7.4)}$ is the fraction of ionized drug at pH 7.4 which can be determined from its pKa.

Results and Discussion

Interaction Studies with Micelles Modelling Intestinal Absorption Enhancers

The NaDC is a well-known bile salt surfactant present in intestinal fluids of GI tract, which tends to form micellar structures aiding the passive absorption of compounds.[54] The benefits of using NaDC to predict human intestinal absorption were described by Waters et al.[54] The distribution of AntiOxCIN$_3$ in the NaDC micellar system, expressed as $LogK_{d(NaDC)}$, was directly determined from the absorption spectra as the spectral interference of these systems only presents residual scattering (Figure S1).[21] Plotting the absorbance values at the maximum absorbance (337 nm) as

a function of NaDC micelles concentration and applying a non-linear fitting (Equation 1), a $LogK_{d(NaDC)}$ of 1.79 ± 0.56 was obtained. This value indicates a good solubilization of AntiOxCIN$_3$ at small intestine level that is facilitated by the presence of the intestinal micelles. Additionally, in silico calculations showed that AntiOxCIN$_3$ has 4 hydrogen bond acceptors and donors, a PSA value of 72.47 Å^2 and a molecular weight of 619.25 Da. Following a relation described by Waters and co-workers,[54] it is possible to estimate that 99% of AntiOxCIN$_3$ will be absorbed at human intestinal level. Understandably, the pH variability of GI can influence the absorption and bioavailability of the drug.[16] However, it is expected a good absorption along all the GI tract, since AntiOxCIN$_3$ distribution in mimetic membrane/aqueous system was not dependent on pH changes (Table S1). The data is reinforced by the PSA value of AntiOxCIN$_3$, as PSA < 140 Å^2 has been described as a prerequisite for drug absorption.[55] The intestinal absorption process involves the transport of the drug through the tight junctions of the intestinal epithelial and can occur by paracellular or transcellular processes, in which physicochemical properties are determinant.[56] The molecular weight limit for paracellular pathway is approximately 400–500 Da,[56] whereby compounds with higher molecular weights are described to permeate trough intestinal epithelium by transcellular processes.[57] Accordingly, the results obtained suggest that AntiOxCIN$_3$ has the physicochemical properties required for an effective passage through the GI tract and into the systemic circulation by transcellular pathway. As expected from a lipophilic compound, and as predicted from the biliary micelle mimetic systems, the absorption of AntiOxCIN$_3$ might be enhanced in the presence of food due to micellar solubilization by the bile salts, uptake by the chylomicrons and lymphatic absorption.[58,59]

Plasma Protein Binding Studies

In systemic circulation, AntiOxCIN$_3$ will be exposed to plasma proteins, like HSA. HSA is a globular protein, and its main physiological function is to transport endogenous and exogenous substances.[60] Drug binding to HSA results in a complex that cannot be transported through epithelium tissue of blood capillaries, limiting the drug distribution to the therapeutic targets.[60,61] Therefore, the drug biodistribution in target tissues is largely affected by its binding to serum proteins and the evaluation of drug-HSA binding is paramount to understand if the drugs' biodistribution is effective.

HSA has three intrinsic fluorophores: tryptophan (Trp), tyrosine (Tyr) and phenylalanine (Phe) and changes in HSA fluorescence are associated with its interaction or binding to a variety of quenchers.[62–65] As observed in Figure 2A, HSA fluorescence emission decreases with increasing concentrations of AntiOxCIN$_3$, with a shift to higher wavelengths (from 334 to 352 nm). Emission spectral shifts can be used to estimate the surrounding hydrophobicity of the chromophore, since the fluorescence emission is strongly dependent on the local microenvironment.[45]

Moreover, the stronger is the polarity the larger will be the solvent relaxation effect resulting ultimately in a longer emission wavelength.[45] So, the observed shift is indicative of an increased polarity surrounding AntiOxCIN$_3$ that can result from protein conformational changes or from the establishment of hydrogen bonds between AntiOxCIN$_3$ and HSA. Similarly, to caffeic acid the hydrogen bonding may take place between the hydroxyl groups of AntiOxCIN$_3$ and the polypeptide chain of albumin.[66] Additionally, by the deconvolution of HSA emission spectra (Figure 2B), it was possible to observe that increasing AntiOxCIN$_3$ concentrations promoted the deactivation of Tyr emission and a bathochromic shift of Trp emission band from 341 nm to 352 nm.

The conformational changes of HSA upon AntiOxCIN$_3$ addition were evaluated by monitoring the synchronous fluorescence intensity of protein residues. By setting a $\Delta\lambda$ value between excitation and emission wavelengths at 15 or 60 nm, it is possible to obtain the characteristic information about Tyr and Trp residues, respectively.[47]

In Figure 2 it is possible to observe that both Tyr (Figure 2C) and Trp residues (Figure 2D) were quenched with increasing AntiOxCIN$_3$ concentrations, indicating that the HSA conformation has been changed. The AntiOxCIN$_3$ addition promoted a small shift of maximum emission band from 275 nm to 277 nm in the Trp spectra (Figure 2D), indicating that the microenvironment around Trp was perturbed and the hydrophobicity decreased. On the other hand, the blue shift on the maximum emission of Tyr (Figure 2C) from 284 nm to 282 nm, indicates that the residues were exposed to a more hydrophobic environment.[67]

Next, similarly to other reported studies,[68,69] a fluorescence quenching study was performed at different temperatures to gain insight into the molecular mechanism of AntiOxCIN$_3$-HSA complexation and to explain the observed microenvironmental changes. The percentage of fluorescence quenching was represented as a function of AntiOxCIN$_3$ concentration for each temperature (Figure S2A). Upon

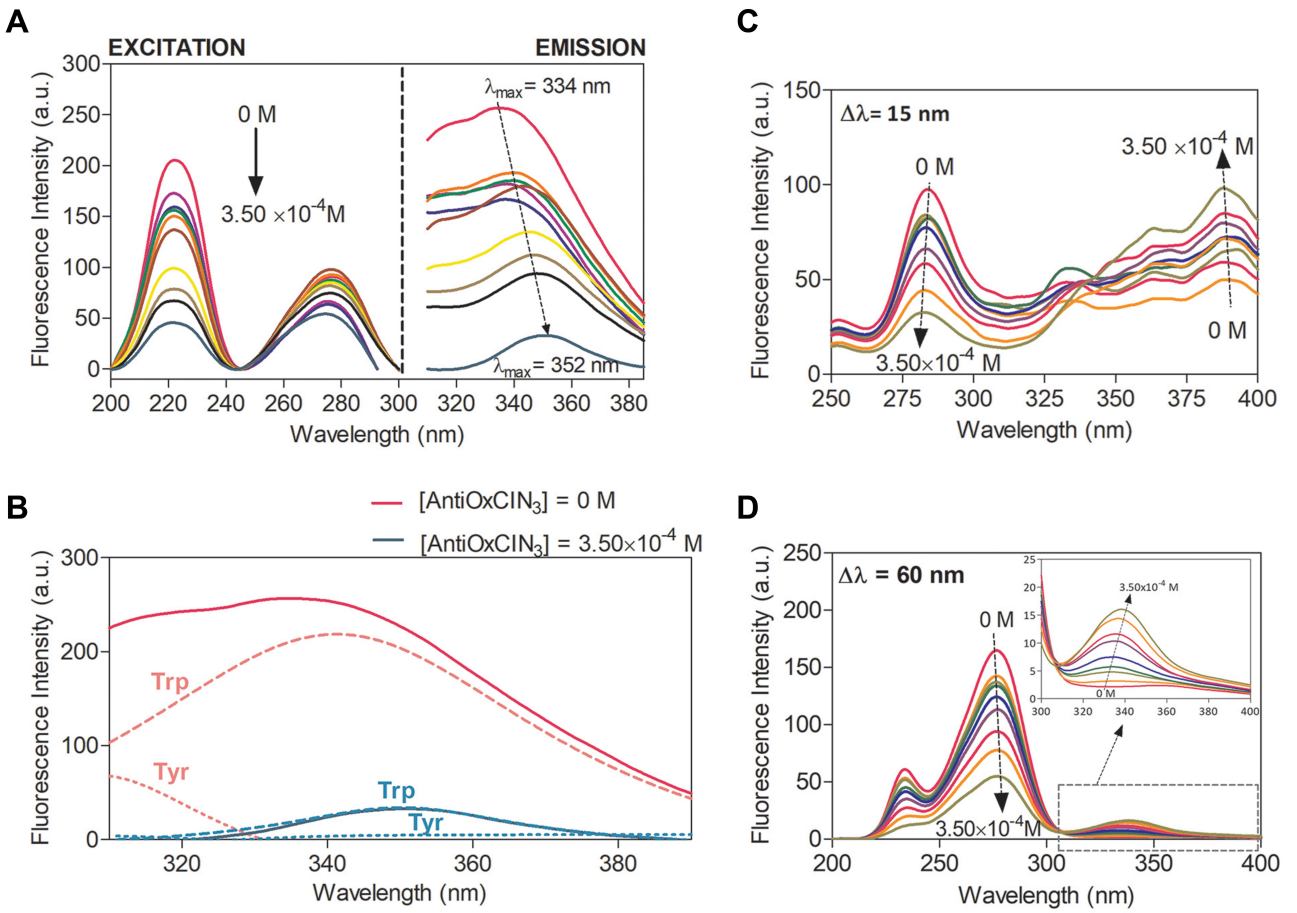

Figure 2 (**A**) Fluorescence spectra of HSA (2.0×10^{-6} M) in the presence of increasing $AntiOxCIN_3$ concentrations (0 to 3.5×10^{-4} M) at 37 °C. (**B**) Deconvolution of HSA Trp (long dashes) and Tyr (short dashes) residues emission bands in the absence (pink) and in the presence (blue) of 3.5×10^{-4} M of $AntiOxCIN_3$. (**C**) Synchronous fluorescence spectra of HSA (2.0×10^{-2} M) in absence and in presence of increasing concentrations of $Anti\text{-}OxCIN_3$ (0 to 3.50×10^{-4} M) with $\Delta\lambda$ = 15 nm corresponding to Tyr residues and (**D**) $\Delta\lambda$ = 60 nm corresponding to Trp residues.

a non-linear fitting (Equation 6) of the fluorescence quenching data, K_{diss} values in the magnitude of 10^{-5} M and K_{bind} values in the magnitude of 10^4 (Equation 7) were obtained for all the temperatures. From K_{bind} values it was determined a *PPB* of 94.76% (Equation 8) meaning that a major part of $AntiOxCIN_3$ in solution is bound to HSA leaving only 5.24% of the free $AntiOxCIN_3$ available to be distributed to the tissues.[46] The magnitude of these values is indicative of a strong interaction between $AntiOxCIN_3$ and HSA.[45] Additionally, from the application of a linear fit of data according to van't Hoff equation (Figure S2B), the thermodynamic parameters of the interaction were determined (Equations 9 and 10). The negative value of ΔG (−26.02 $KJ{\cdot}mol^{-1}$) suggests a spontaneous HSA-$AntiOxCIN_3$ complexation.[70] Furthermore, the positive values of ΔH (4.35 $KJ{\cdot}mol^{-1}$) and $T\Delta S$ (0.03 $KJ{\cdot}mol^{-1}{\cdot}K^{-1}$) clearly indicate that the binding is entropically driven.[71] According to Ross's thermodynamic laws for the binding between small molecules and biomacromolecules, this type of entropic control of the binding process indicates that the hydrophobic interactions may play a predominant role in HSA-$AntiOxCIN_3$ association.[70]

Gathering all the outcomes provided by fluorescence methods it was possible to predict a hydrophobic interaction between $AntiOxCIN_3$ and the Tyr residue of HSA with a consequent protein conformational change that promotes the exposure of Trp residues to aqueous solution. As for caffeic acid, the aromaticity of the $AntiOxCIN_3$ molecule might play an important role in hydrophobic interactions established between the phenyl group of $AntiOxCIN_3$ and hydrophobic aminoacid residues present within the protein binding site.[66]

Additionally, to confirm the interaction, R_h and zeta-potential of free and complexed HSA with $AntiOxCIN_3$ were measured by DLS and ELS, respectively, and the results obtained are summarized in Figure 3.

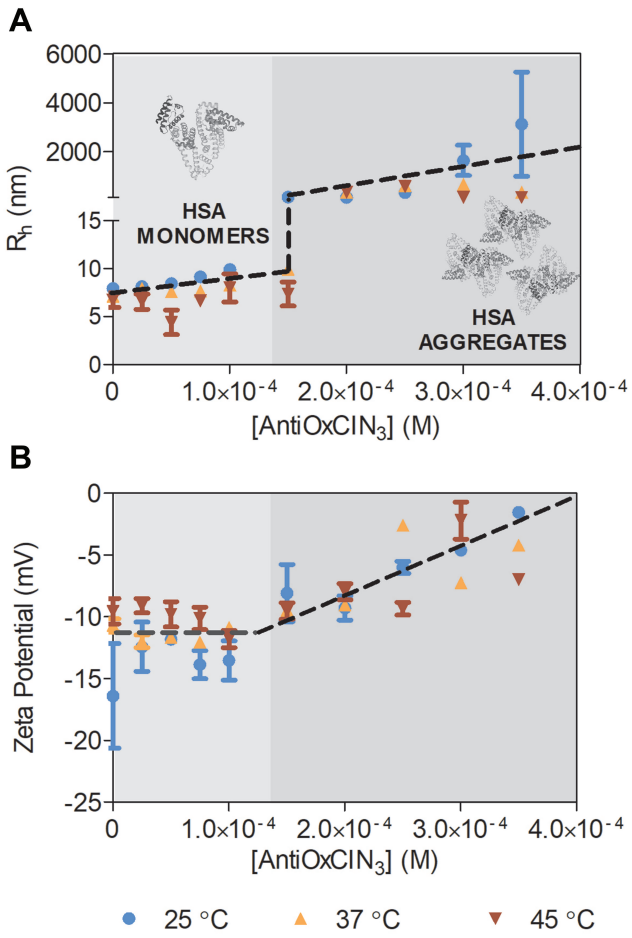

Figure 3 Graphic representation of R_h obtained from DLS (**A**) and Zeta Potential values (**B**) for HSA and HSA-AntiOxCIN$_3$ ([AntiOxCIN$_3$] from 0 to 3.50×10^{-4} M), at three different temperatures represented by different colors and signs. The black dashed line shows the tendency for neutralization upon AntiOxCIN$_3$ addition observed by increase values of R_h and zeta potential.

In the absence of AntiOxCIN$_3$, the R_h of HSA was determined to be 7.97 nm, 7.13 nm and 6.75 nm, at 25.0, 37.0 and 45.0 °C, respectively. The data is coherent with the size range of HSA described in the literature.[72] The progressive increasing of AntiOxCIN$_3$ concentration provoked an increase in R_h values, suggesting the formation of the complex AntiOxCIN$_3$–HSA (Figure 3A). Remarkably, at 2.0×10^{-4} M of AntiOxCIN$_3$ a significant increase in the R_h value was observed, coinciding with the concentration at which the maximum fluorescence quenching was reached (Figure S2A). The large increase in R_h values suggests that HSA has reached the saturation binding point, promoting protein aggregation.

The ELS studies showed negative surface charge for free HSA, however, a charge neutralization tendency occurred upon AntiOxCIN$_3$ addition (Figure 3B). This tendency resulted in reduced electrostatic repulsions which explain the formation of larger aggregates. These results corroborate the exposure of neutral Trp residues to the solvent upon AntiOxCIN$_3$ interaction with Tyr residue, as predicted by fluorescence studies. Indeed, the progressive surface exposure of neutral residues will decrease the negative charge density of the protein, which justifies the observation of less negative zeta potential values, and ultimately less repulsion and higher tendency for aggregation.

As stated before, the evaluation of the binding parameters between plasma protein and drug candidates is an important factor to understand their distribution from the human plasma to body tissues and organs. Therefore, although intestinal absorption of AntiOxCIN$_3$ is feasible, its distribution to the target tissues can be limited, by the strong binding to HSA (AntiOxCIN$_3$ has a *PPB* of 94.76%). However, the strong binding to HSA cannot by itself be considered a final decisive factor for a poor biodistribution profile. Changes in protein binding may occur in vivo, for example, by competitive displacement between co-administration of drugs that share the same binding site.[73] In addition, the binding of many drugs to HSA in patients can be changed due to several disease conditions (eg, kidney and liver diseases).[73] Finally, it has been suggested that compounds with logD >3 and high *PPB* have an increase absorptive GI permeability, as the binding to albumin improves circulation and decreases the cellular accumulation, which may also lead to limited efficiency of drug's intestinal metabolism.[74] Therefore, AntiOxCIN$_3$ may benefit from these effects being well absorbed orally, similarly to what has been predicted for related compounds, like MitoQ.[74]

Interaction with Lipid Nanosystems Used as Cell Membrane Mimetic Models

The ability of a drug to permeate the cell membranes through the phospholipid polar head region, diffusing through the lipophilic hydrocarbon chains and emerging into the inner region of phospholipid polar headgroups is determinant for its body distribution.[18,75] The ability of AntiOxCIN$_3$ to interact with membranes depends on an appropriate balance between liposolubility and hydrosolubility, which in turn is determined by its lipophilicity.[16] Although lipophilicity is usually expressed as a partition of the drug in the octanol/water system, lipid membrane/water partition models, such as the PC model, are receiving increased attention as they can better predict drug

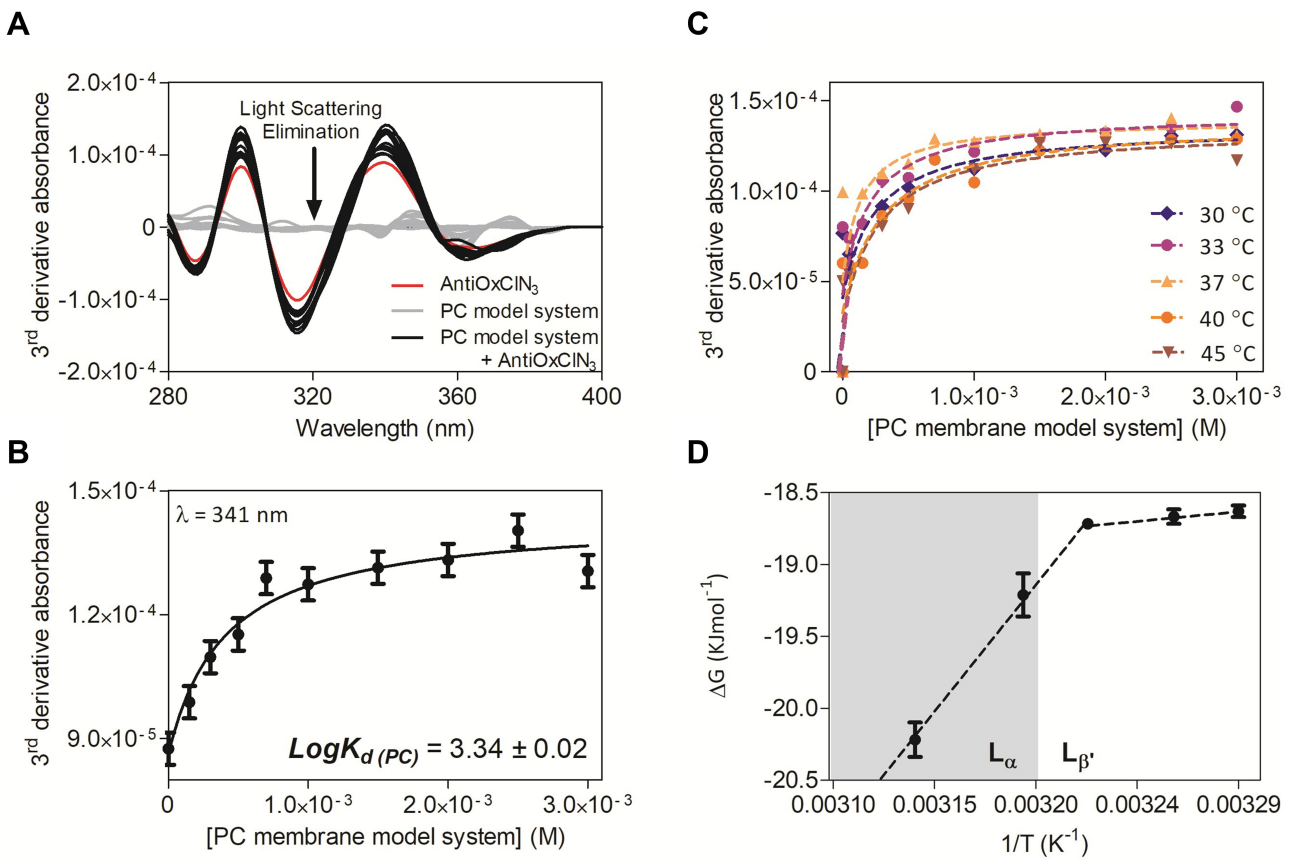

Figure 4 PC membrane model system partition coefficient of AntiOxCIN$_3$ by derivative spectrophotometry: (**A**) Third derivative of AntiOxCIN$_3$ (2.0×10^{-4} M) absorption spectra in aqueous buffered phase pH=7.4 (red), after incubation with PC membrane model system (0–3.0×10^{-3} M) (black) and PC membrane model system in the absence of AntiOxCIN$_3$ (grey); (**B**) Non-linear fitting by Equation 1 of derivative absorbance at λ=341 nm as a function of PC membrane model system concentration. (**C**) Third derivative of the absorbance spectra and respective non-linear fitting by Equation 1 (dashed line) at several temperatures; (**D**) van't Hoff plot representing the Gibbs free energy values as function of the inverse of temperature, in K^{-1}, with the transition temperature between gel ($L_{\beta'}$) and fluid (L_{α}) lipid phases highlighted.

biodistribution.[15,34,48,76] In this regard, the concentration of the drug distributed in each phase of the binary lipid/water system can be determined by UV-VIS spectrophotometry.[44] Increasing concentrations of PC membrane model system promoted light scattering in the absorbance spectra of AntiOxCIN$_3$, which results in increased baseline values. Derivative method was applied to eliminate the background signals' effect and to improve the resolution of overlapping bands (Figure 4A).[21,34,44]

Thus, fitting the experimental data with Equation 1 (Figure 4B) at wavelengths where the scattering is eliminated (Figure 4A), a mean $LogK_{d(PC)}$ = 3.34 ± 0.02 (pH 7.4) was obtained. This value indicates a moderate to high lipophilicity ($0 < LogK_d < 5$) and is characteristic of a drug with a good balance between solubility and permeability, which can be translated as optimal for cell membrane permeation and low metabolic liability.[16,77]

Additionally, AntiOxCIN$_3$ has shown similar values of $LogK_{d(PC)}$ in a wide pH range (Table S1). The lipophilicity properties of AntiOxCIN$_3$ influence its biodistribution and bioaccumulation.[16] Considering the $LogK_{d(PC)}$ obtained by derivative spectroscopy as representative of the distribution in cell membranes of different organ/tissue, it was possible to estimate AntiOxCIN$_3$ bioaccumulation sites ($K_{bioaccumulation}$ determined using Equation 15). In general, AntiOxCIN$_3$ is likely to bioaccumulate at more peripheral tissues: adrenal glands (61.44%), thyroid (30.72%) and kidneys (3.07%).[16]

Besides the estimated bioaccumulation of AntiOxCIN$_3$ in off-target tissues, its *ASI*, that accounts for the partitioning of the drug in the adipose tissue, was determined to be 3.105 ± 0.016 (Equation 16), suggesting a high distribution in these tissues comparable to other neutral drugs such as clobazam.[49]

Additional biodistribution parameters were also determined using the values of *PPB* to HSA and $LogK_{d(PC)}$ obtained. The unbound AntiOxCIN$_3$ fraction in plasma and tissues were respectively determined as f_u=0.052

(Equation 20) and f_{ut}=0.011 (Equation 21). These parameters were used to obtain VD_{SS}=1.89±0.43 L·Kg^{-1} (Equation 19), which agrees with the *ASI* value obtained. Indeed, drugs with VD_{SS} values between 1 and 5 L·Kg^{-1} are characterized as having large volumes of distribution due to affinity for adipose tissues which hampers their elimination from the body.[78] In fact the tendency to accumulate in adipose tissues and the large VD_{SS} prolong the half-life of the compound, reducing its elimination rate.[79] A large VD_{SS} also means that the compound is more difficult to eliminate from the body by extracorporeal removal therapies (eg, dialysis).[80]

Lipophilicity is the net result of all intermolecular forces (hydrophobic, polar and/or ionic interactions) involved in the drug partition between two phases of different polarity.[15] For the thermodynamic characterization of the intermolecular mechanisms involved in the distribution of AntiOxCIN$_3$ in membranes, the $LogK_{d(PC)}$ was determined at five different temperatures (Figure 4C). The values are summarized in Table S2. The graphic representation of ΔG values as function of 1/T (K^{-1}) (Figure 4D where data was fitted using Equations 9 and 10) evidenced a spontaneous process ($\Delta G < 0$) with a biphasic behavior. The variation of enthalpy and entropy are related with the energetic requirements and the molecular randomness (increase or decrease in the molecular disorder), respectively, implied in AntiOxCIN$_3$ transfer from the aqueous phase to the lipid media. When the lipid membrane model is in the fluid phase, both variations of enthalpy and entropy have positive values (ΔH= 43.9 KJ·mol^{-1} and $T\Delta S$= 0.200 KJ·mol^{-1}), suggesting the presence of hydrophobic interactions between AntiOxCIN$_3$ and PC membrane model system.[70] However, when the lipid membrane is in the gel phase, the negative variation of enthalpy and positive entropy variation (ΔH = −14.9 KJ·mol^{-1} and $T\Delta S$ = 0.012 KJ·mol^{-1}) were indicative of the presence of strong van der Walls interactions. The biphasic behavior presented in Figure 4D suggests that with the temperature increase, the microviscosity and order of membrane decreased, which led to a better membrane penetration of AntiOxCIN$_3$. This is also corroborated by the higher negative values of free binding energies, which indicate greater affinity of the ligand to the membrane lipid network.[81] Additionally, from the gel phase to the fluid phase, a significant increase in enthalpy variation occurred indicating that intermolecular forces are stronger in the fluid phase and suggesting an entropically driven distribution of AntiOxCIN$_3$ in the membrane model system.[70] Moreover, considering that at physiological temperature (37 °C) cell membranes are mostly in the fluid phase (with more ordered domains confined to the lipid rafts),[82] it can be concluded that AntiOxCIN$_3$ tends to establish hydrophobic interactions with cell membranes in an entropic driven and spontaneous process.

To assess AntiOxCIN$_3$ location in the membrane system, four probes, covering both polar and hydrophobic core of the membrane bilayer, containing the same fluorescent group located at different and well-defined depths of the bilayer (n-AS, where n= 3, 6, 9 and 12) were used.[21,45] The ability of AntiOxCIN$_3$ to quench each probe was monitored to obtain information about how deeply AntiOxCIN$_3$ was buried within the bilayer structure.[21] As the $LogK_{d(PC)}$ values of AntiOxCIN$_3$ in lipid phase were previously determined, the effective concentrations of AntiOxCIN$_3$ in the membrane model system – [AntiOxCIN$_3$]$_M$ – are calculated using Equation 3.[21] In Figure 5A, it can be observed that all quenching processes involved a static mechanism since the slope of the τ_0/τ linear plot was nearly one. Static and collisional quenching can also be distinguished by their varying temperature dependence (Table S3). When K_{sv} values increase with the temperature, there is an indication of collisional quenching because higher temperatures result in faster diffusion. In this case, higher temperatures resulted in lower K_{SV} values as a result of the decoupling of the complex formed between the probes and AntiOxCIN$_3$. Therefore, from the analysis of the quenching process one can conclude that the quenching occurred by a static mechanism.

Using Equation 2, K_{SV} values were determined from the slopes of the linear plots of the probes 6, 9 and 12-AS (Figure 5A). A deviation from linearity was observed in the Stern–Volmer representation of steady-state data related with the fluorescence quenching of 3-AS probe (Figure 5A). When the deviation is in form of an upward curvature generally it means that the extent of quenching can be explained by two types of quenching mechanisms: collisional encounters and static binding between quencher and probe.[40,45] However, in our case there is no collisional mechanism of quenching because the slope of the τ_0/τ linear plot was nearly one and K_{sv} decreases with temperature increase. Importantly, downward curvatures were observed in charged quenchers upon binding to the probe (in this case the TPP cation is closely located to the carboxylate anion from the stearic acid of 3-AS probe). Therefore, the analysis of the quenching process

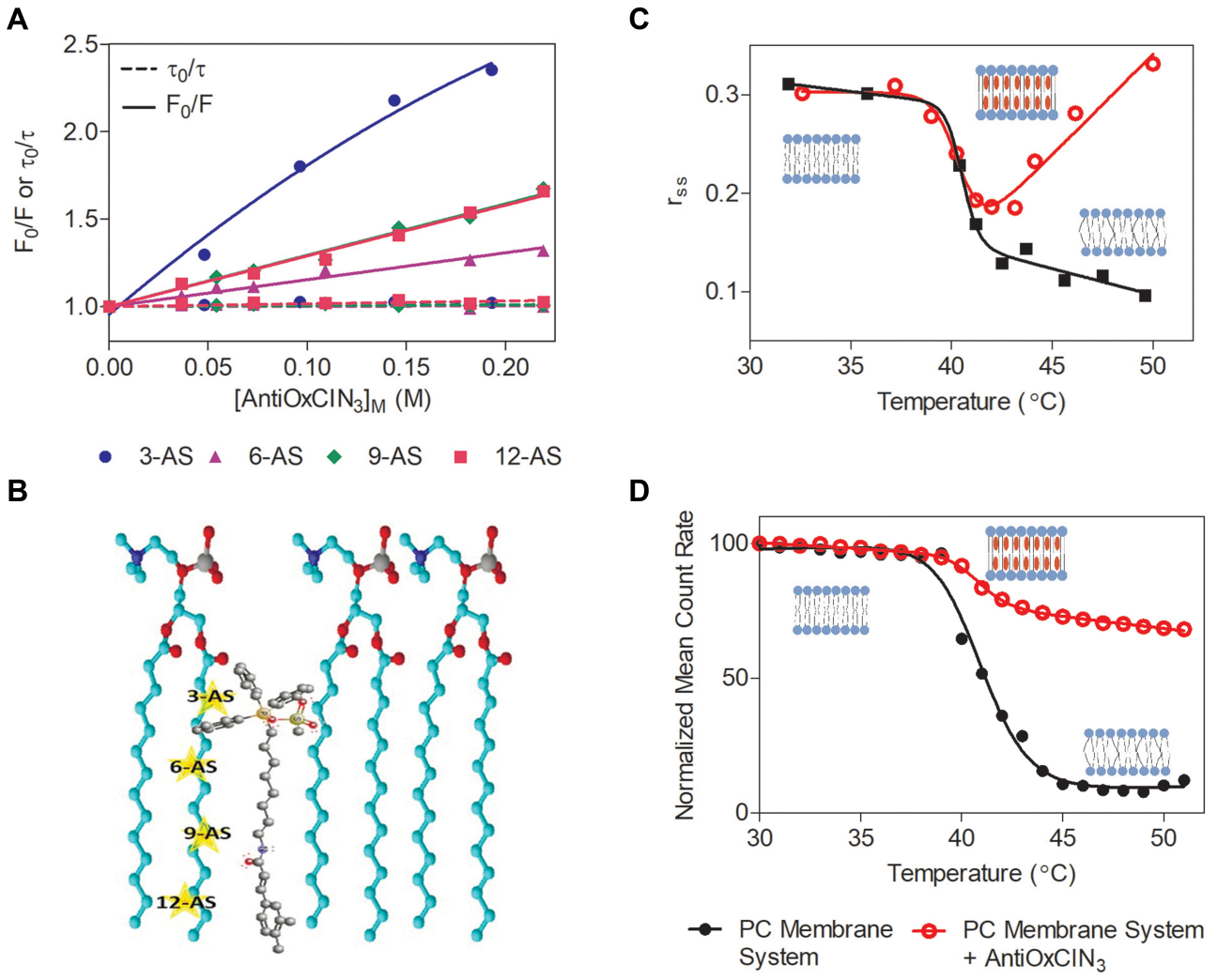

Figure 5 (**A**) Stern-Volmer plots of the probes n-AS incorporated in the PC membrane system at 37 °C as a function of AntiOxCIN$_3$ ([AntiOxCIN$_3$]$_M$). Different colors and signs represent the different probes used. The full line represents the linear fitting applied to steady-state data. The dashed line represents the linear fitting applied to the data obtained from lifetime measurements. (**B**) Schematic representation of the possible location of the n-AS (n=3, 6, 9 and 12) fluorescent probes and AntiOxCIN$_3$ within PC molecules of the PC membrane system. Membrane microviscosity assessment studies in the presence (red) and absence (black) of AntiOxCIN$_3$ and respective sigmoidal fits: (**C**) Anisotropy, r_{ss}, profile of DPH probe in the PC membrane model system dependent on the temperature with fitting using Equation 3; (**D**) Sigmoidal profile of normalized mean count rate (MCR) obtained by DLS as function of temperature with sigmoidal fit using Equation 14.

indicates a quenching occurring by a static mechanism, which suggests the existence of binding between 3-AS probe and a quencher group present in AntiOxCIN$_3$. Consequently, it is possible to calculate K_{SV} as an equilibrium binding constant (ie, the inverse of dissociation constant, K_{diss}, determined by fitting data according to a nonlinear regression model described in Equation 6). From the K_{SV} values and using Equation 4, K_q values were obtained for all the probes and summarized in Table 1.

From the data acquired, it was concluded that AntiOxCIN$_3$ was able to quench all the probes, with a more noticeable fluorescence quenching at 3-AS probe level. From the K_q values obtained, it is possible to establish a correlation with the quencher moieties present in AntiOxCIN$_3$ and propose the most probable orientation of the drug in the lipid membrane. Considering the different chemical groups present in AntiOxCIN$_3$ structure, aromatic rings display higher ability to quench the

Table 1 Fluorescence Quenching Constants Obtained from Measurements of Fluorescence Quenching Studies for n-AS Fluorescence Probes in PC Membrane Model System at 37°C

Probe	3-AS	6-AS	9-AS	12-AS
K_{SV} (M^{-1})	11.25	1.54	2.99	2.90
K_q ($M^{-1}\cdot s^{-1}$)	1.36×10^6	1.73×10^5	2.71×10^5	2.52×10^5

Abbreviations: K_{SV} Stern-Volmer constant; K_q, bimolecular quenching rate constant.

fluorescence emission of the probes. Hence, it is possible to predict an extended molecular orientation of AntiOxCIN$_3$ parallel to the long axis of the phospholipid acyl chains, as represented in Figure 5B. The data agrees with the values of the high lipophilicity determined.

Once AntiOxCIN$_3$ is deeply inserted into the membrane, it is crucial to understand how this compound can influence the physicochemical and biophysical state of the membrane bilayer. Parameters such as membrane fluidity and phospholipid order and/or packing play a key role in the maintenance of membrane dynamics that supports the most basic cellular functions[21] and changes induced by drugs in these parameters can provide valuable information on their therapeutic ability and possible toxic effects at membrane level. Membrane microviscosity changes upon addition of drugs are usually monitored by steady-state fluorescence anisotropy.[21] Steady-state anisotropy (r_{ss}) changes are related to the alterations in the rotational movement of the probe caused by differences in the stiffness of its surrounding matrix.[21,34] Therefore, the r_{ss} of DPH probe was used to study the effect of AntiOxCIN$_3$ on membrane's fluidity (Equation 5). DPH locates at the hydrophobic region of the lipid bilayer, reporting the microviscosity of the acyl chains close to the center of the bilayer.[83] In the gel phase (L_β), the r_{ss} of DPH in PC membrane models was found to be between 0.32 (at 22.2 °C) and 0.23 (at 40.4 °C), and a lipid main phase transition to the fluid phase (T_m $L_\beta \rightarrow L_\alpha$) occurred at 40.6 °C (Figure 5C black data). In the L_β phase, the AntiOxCIN$_3$ addition did not cause any significant change, since the r_{ss} values of the PC system with the drug were found to change between 0.33 (at 29.0 °C) and 0.24 (at 40.3 °C), presenting a T_m $L_\beta \rightarrow L_\alpha$ at 40.5 °C (Figure 5C red data). As expected, in the L_α phase, the r_{ss} of DPH in PC membrane model assumes lower values from 0.17 (at 41.2 °C) to 0.09 (at 55.7 °C). However, upon AntiOxCIN$_3$ addition, these values increase to 0.19 (at 41.2 °C) and to 0.38 (at 54.0 °C). The surprising large increase of r_{ss} values promoted by AntiOxCIN$_3$ reflects a higher lipid packing of the membrane model system in a deeper region where DPH is inserted. This is possibly due to AntiOxCIN$_3$ intercalation in the hydrophobic region of the bilayer, as predicted by the location studies, and by the hydrophobic interactions that AntiOxCIN$_3$ established with the phospholipids.

During the lipid phase transition there are distinct ordered phases,[84] which are able to scatter light with different intensities. Accordingly, it is possible to monitor, within a temperature range and using DLS, the average number of photons scattered (mean count rate, MCR) by the lipid membrane system.[85] This type of measurement results in a sigmoidal profile as the one presented in Figure 5D. Applying Equation 14 to the acquired data, it was possible to determine B, in the absence and presence of AntiOxCIN$_3$, as 589.9 and 901.1, respectively. B is intimately connected with the mean size of the ordered or fluid lipid regions that can exist at different transition stages. In practical terms, a high cooperative transition is characterized as a transition where the fluid regions increase very rapidly with a simultaneous fast decrease of ordered regions, while in a less cooperative system there is a co-existence of fluid and ordered regions on an appreciable range.[84] Additionally, although the T_m $L_\beta \rightarrow L_\alpha$ remained constant, there was a clear difference in the fluid phase between the PC lipid system without and with AntiOxCIN$_3$. The AntiOxCIN$_3$ addition provoked a clear increase in the number of photons detected in the fluid phase of PC lipid system, reflecting an increased stiffness when compared with PC membrane system without AntiOxCIN$_3$.[85] This observation corroborates the membrane stiffness effect observed by steady-state anisotropy studies. Thus, considering the gathered outcomes obtained by two different techniques, it was possible to conclude that AntiOxCIN$_3$ addition to the PC membrane system promoted the formation of a tightly packed lipid structure.

The influence of AntiOxCIN$_3$ on the biophysical properties of membranes, such as long-range bilayer order and hydrocarbon chain packing, was explored by SAXS and WAXS. In the L_β phase, the SAXS pattern obtained for fully hydrated PC lipid system showed three Bragg peaks with characteristic positions of lamellar phases. Upon AntiOxCIN$_3$ addition, the three Bragg peaks disappeared, originating a broader single peak (Figure S3). The less intense and broader Bragg peak revealed a disturbing effect of AntiOxCIN$_3$ in the lipid structure. From the first-order Bragg peak of each lipid phase, long spacing (d_L) and correlation length between bilayers (ζ) were determined (Equations 11, 12 and 13). The obtained profiles of d_L values in the presence and absence of AntiOxCIN$_3$ as function of temperature are represented in Figure S3. These profiles indicated that for all the temperatures d_L increased upon AntiOxCIN$_3$ addition. In fact, the incorporation of AntiOxCIN$_3$ promoted an increase of the bilayer thickness up to approximately 20 Å, in the L_β phase, and 30 Å, in the L_α phase. This substantial increase can result from changes in the hydration behavior and/or from an alteration in

phospholipid headgroups orientation, with reduction of the tilt angle of the chains, due to interaction with AntiOxCIN$_3$. According to Fernandes et al,[21] a difference of 6.1 Å in the bilayer thickness is expected when the loss of tilt angle of hydrocarbon chains occurs. However, the changes observed in the tilt angle alone are not enough to explain the increased d_L observed due to the incorporation of AntiOxCIN$_3$, which means that an increase in the hydration layer is likely to occur along with the changes in the tilt angle. Additionally, the deconvolution of the first-order Bragg peak in the presence of AntiOxCIN$_3$ (Figure S3) showed a non-influenced phase (d_L similar to that of pure PC membrane system) and an influenced phase (d_L higher than pure membrane system). The incorporation of AntiOxCIN$_3$ into PC membrane systems is responsible for pronounced changes in ξ values. In PC membrane system, diffraction peaks presented high ξ values – 13,291 Å (in the L_β phase) and 8763 Å (in the L_α phase) – which indicated a good correlation between bilayers. When AntiOxCIN$_3$ was added, these values decreased to 574 Å (in the L_β phase) and 895 Å (in the L_α phase), which is indicative of a disturbing effect in the global molecular organization of the multilayer stack of lipid bilayer.

From the WAXS patterns obtained for PC membrane system (Figure 6A), a single symmetric Bragg peak was observed that allowed determining a short spacing d_S value around 4.13 Å (Equations 11 and 12), characteristic of a hexagonal chain packing and a cross-sectional area of 19.65 Å^2.[2,26] The high ξ value (Equation 13) obtained (1718 Å) indicated a good correlation between bilayers. As

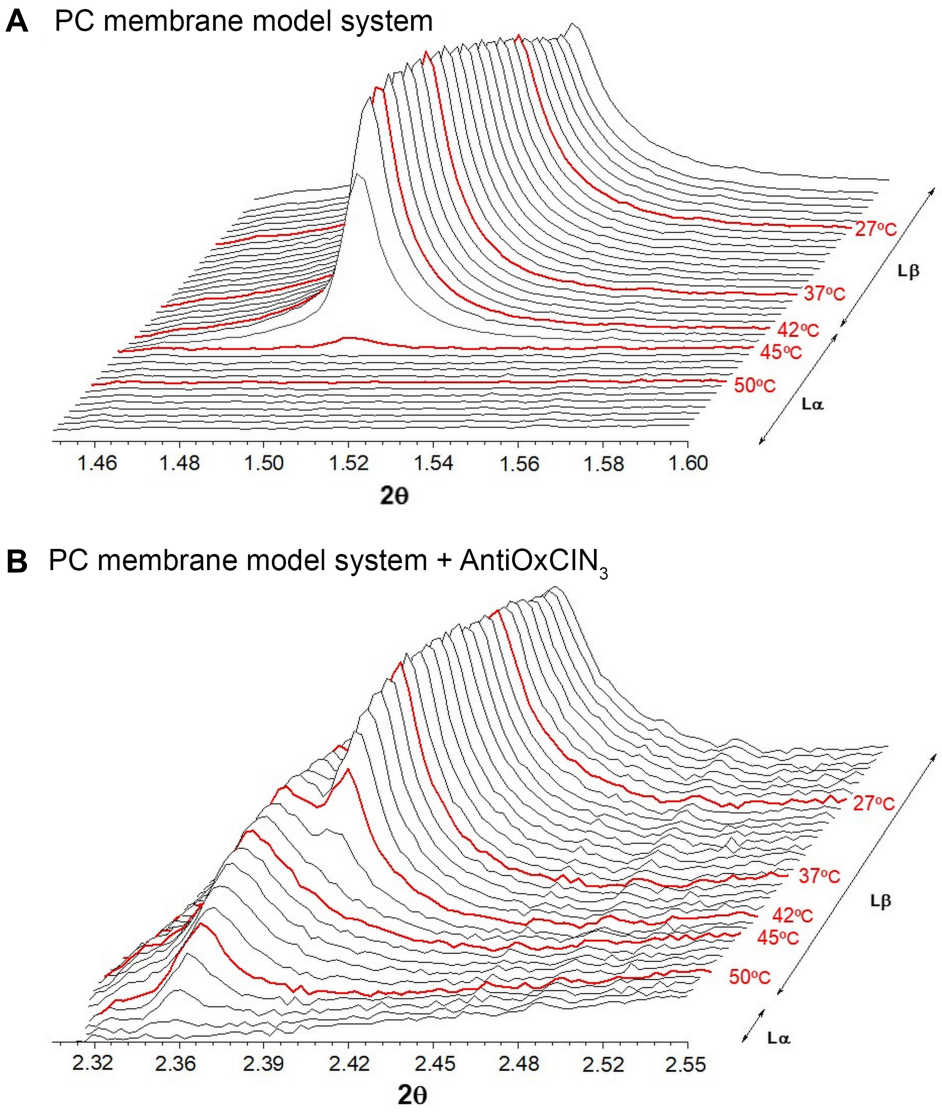

Figure 6 WAXS patterns of PC membrane system in the absence (**A**) and presence (**B**) of AntiOxCIN$_3$ with some temperatures highlighted in red.

expected, after T_m $L_\beta \rightarrow L_\alpha$ (T>45 °C) there was no Bragg peak in the WAXS region since the lipid bilayers were in the fluid phase. Upon AntiOxCIN$_3$ addition, the symmetric Bragg peaks gave rise to a double asymmetric Bragg peak with short spacings characteristic of a pseudo-hexagonal lattice of the chains in the bilayers (d_{20} = 4.14 Å and d_{11} =4.18 Å) and a cross-sectional area of 19.93 Å^2 (Figure 6B).

The intercalation of AntiOxCIN$_3$ reduced the ξ (ξ = 471 Å), suggesting a disturbing effect in membrane multilayer structure. For T>45 °C, where no Bragg peaks were expected to appear (due to the fluidization of the lipid bilayer), it was still visible an asymmetric single Bragg peak, with d_s≈4.23 Å and a cross-sectional area of 20.81 Å^2, which only disappeared at T>50 °C (Figure 6B). The results obtained by a third different technique corroborate the membrane stiffening effect caused by AntiOxCIN$_3$ which was also observed by the other two techniques (DLS and steady-state anisotropy). As suggested by the thermodynamic studies, AntiOxCIN$_3$ establishes hydrophobic interactions with membrane phospholipids. These interactions might be the cause for the membrane stiffening effect observed. Finally, the observed increase of lipid cross-sectional area upon AntiOxCIN$_3$ addition indicates the penetration of the drug within the aliphatic core of the membrane confirming its intercalation between the hydrophobic lipid chains observed in the location studies.

BBB Membrane Interaction Studies

Drug delivery to the CNS represents a challenging task due to the presence of the BBB. It is one of the most important blood–CNS interfaces, protecting the brain from potentially harmful xenobiotics while simultaneously regulating the transport of essential molecules and maintaining a stable milieu for neuronal function.[86] The BBB gatekeeper function is essentially a result of the endothelial cells lining the brain capillaries sealed together by an intricate network of tight junctions, which restrict severely the transport of the drugs. Since one of AntiOxCIN$_3$ potential therapeutic targets is the CNS, where the new chemical entity can exert its antioxidant effect, it is important to predict its ability to permeate through BBB. Therefore, the BBB endothelial cellular membranes were mimicked by a lipid nanosystem composed of brain phospholipids (BPL) and used as model to predict how AntiOxCIN$_3$ interacts with BBB lipid barrier. This interaction can be inferred using derivative spectroscopy, as performed in the previous studies (Figure S4). In the third derivative of absorbance spectra an evident bathochromic shift occurred, suggesting changes in polarity of microenvironment surrounding AntiOxCIN$_3$ due to its distribution in the lipid phase. A $LogK_{d(BBB)}$ of 3.64 ± 0.25 (Equation 1) was obtained which is indicative of AntiOxCIN$_3$ tendency to distribute in BBB endothelial cell membrane. Moreover, several mathematical models and/or in silico descriptors can be used to classify a drug accordingly to its BBB distribution. Thus, a drug can be classified as BBB+ or BBB- using the threshold cut-offs described in the literature.[87] From the application of Equation 17, it was possible to determine a *LogBB* of 2.77 ± 0.10, which suggests potential BBB permeability.[88] Moreover, using Equation 18 and considering VWSA$_B$ as 0.59, a *LogPS* of −1.88 was obtained. Bearing in mind the reported cut-off schemes, AntiOxCIN$_3$ is classified as BBB+.[87] Thus, from the interaction studies of AntiOxCIN$_3$ with BBB membrane model system, it is predicted that AntiOxCIN$_3$ can permeate BBB.

Considering the high distribution coefficient of AntiOxCIN$_3$ in the BBB membrane system, SAXS studies were performed in BPL to study the possible order perturbations caused by the drug in this biological interface. The SAXS pattern of BPL in the presence of AntiOxCIN$_3$ presents two Bragg peaks characteristic of a lamellar phase organization at 20 °C with a d_L = 5.83 nm (Figure 7). A high correlation between bilayers (ξ = 8918 Å) was obtained, suggesting that the drug does not disturb the multilayer stack of the lipid bilayer. However, as previously reported,[89] at 20 °C the SAXS pattern of BPL presents a L_α phase with d_L = 9.86 nm that upon heating,

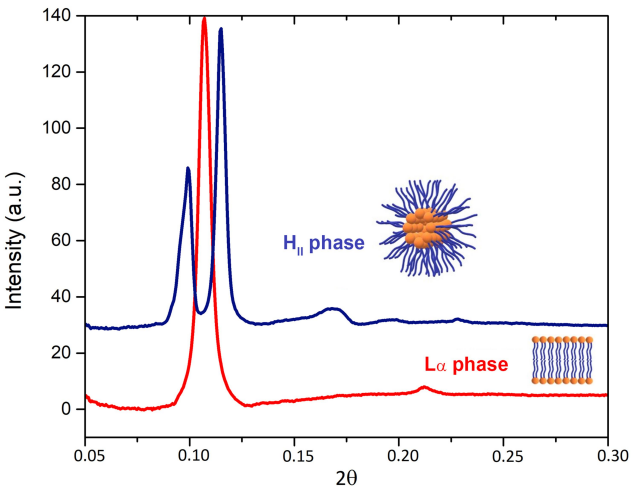

Figure 7 SAXS patterns of a BPL membrane model system in the presence of AntiOxCIN$_3$ before (red line) and after (blue line) the transition between lamellar phase (L_α) to inverted hexagonal phase (H_{II}).

at 40 °C, is converted into an inverted hexagonal phase (H_{II}), with a lattice parameter a=2d/√3=7.72 nm. The 4 nm decrease of d_L value associated with the high correlation between bilayers suggests that AntiOxCIN$_3$ addition provokes a reduction of the hydration layer between the lipid bilayers. Furthermore, upon the addition of AntiOxCIN$_3$ to BPL a H_{II} phase with a lattice parameter a = 7.59 nm is observed already at 30 °C (Figure 6C). The ability of AntiOxCIN$_3$ to significantly decrease the L_α-to-H_{II} phase transition temperature (T_H) is relevant from a therapeutic point of view. Actually, a similar behavior was observed for some natural bioactive fatty acids on lipid membranes.[90,91] The effects of these bioactive fatty acids included the capacity to reduce the blood pressure (H_{II} phase induction has regulatory effects on G protein-associated signaling cascades); antiproliferative effects (H_{II} phase induction promotes the subsequent recruitment of protein kinase C to the cell membrane) and the ability to promote membrane fusion and thus interfere with related cellular processes (endo/exocytosis, cell division).[90] Focusing on the effect of AntiOxCIN$_3$ in BPL, the observed T_H reduction can as well be related to membrane fusion processes[92,93] and to an increase of BBB permeability,[94] however this type of effects must be confirmed by cellular assays in a near future. However, at this point, it is possible to assure that the T_H reduction effect observed by SAXS agrees with the BBB+ classification and supports the assumption that AntiOxCIN$_3$ is able to permeate BBB.

Conclusions

In this study, the drug-like properties of AntiOxCIN$_3$, a novel mitochondriotropic antioxidant previously described by Teixeira et al,[10] were characterized using lipid nanosystems and serum protein as relevant biomimetic interfaces to obtain important information correlated with its in vivo biodistribution.

Our results demonstrated that AntiOxCIN$_3$ is expected to be effectively absorbed in GI tract through transcellular process and reach the bloodstream. At the bloodstream, the compound is predicted to strongly interact with the plasma albumin, with more than 90% of AntiOxCIN$_3$ binding to albumin, causing changes in protein conformation. The high affinity of AntiOxCIN$_3$ to plasma protein is in line with its determined high lipophilicity. Tendency to bioaccumulate in peripheral tissues and adipose tissues is also predicted and corroborated by the VD_{SS} value (1.89±0.43 L·Kg^{-1}). This value is in the range of the drugs often characterized by having a large volume of distribution and a slow rate of elimination from the body. Additionally, AntiOxCIN$_3$ interacts with cellular membranes through hydrophobic forces and tends to be located parallel to the long axis of phospholipid acyl chains. In this interaction there are no signs of major disturbance on the membrane transition temperature and cooperativity which points to the absence of membrane biophysical impairment and thus lack of membrane toxicity. However, the preferred location of the drug at bilayer level explains the observed increase in membrane stiffness confirmed by all the complementary techniques applied (steady-state anisotropy, DLS, SAXS and WAXS). Considering the widespread involvement of oxidative stress in several diseases, including disturbance effects observed at CNS level (eg, brain homeostasis disorders that predispose to neurodegenerative conditions, harmful effects on the expression of important molecules involved in BBB integrity, and apoptosis of pericytes[95]) the predicted ability of AntiOxCIN$_3$ to overcome BBB and exert its antioxidant effect in the brain, is a positive outcome when considering its potential therapeutic use.

As reviewed by Murphy et al,[13] the covalent link of a TPP lipophilic cation to improve the delivery of antioxidants has proven to be an efficient strategy in vivo. In fact, the results reviewed showed that this class of mitochondriotropic antioxidants (in which AntiOxCIN$_3$ is included) are able to pass easily through all biological membranes, including BBB, and showed a tendency to be located at the hydrophobic portion of the lipid/water interface, ie, close to the phospholipids' fatty acyl groups level. The ability of other type mitochondriotropic antioxidants to be absorbed from gut to the bloodstream was also reported.[13] Overall, our results are in accordance with these studies, which reinforces the importance to use biomimetic models as an approach for the prediction of the drug biological behavior, as well as, to understand how the molecular structure might affect such behavior. In this regard, our studies indicate that AntiOxCIN$_3$ might have a good biodistribution profile, being able to be absorbed at GI tract and overcome membrane barriers of off-target tissues and BBB. The only hindrance to the effective biodistribution of AntiOxCIN$_3$ may be its strong binding to HSA. However, this apparent drawback can be tuned with either a structural optimization to reduce AntiOxCIN$_3$ lipophilicity or its encapsulation in stealth nanocarriers systems. On the other hand, the strong HSA binding of MitoQ10 (lipophilic compounds similar to AntiOxCIN$_3$)

has been reported as an advantage to avoid cellular accumulation of compounds leading to limited intestinal metabolic conversion and accelerating absorptive transport.[74]

Regarding the membrane toxicity effects of AntiOxCIN$_3$, they seem to present no concern, as high molar ratios of the drug did not induce relevant membrane impairment, which can cause loss of membrane integrity. The major biophysical effects of this mitochondriotropic antioxidant was its surprising capacity to increase membrane stiffness in the fluid phase and its ability to facilitate H_{II} phase in BBB endothelial membrane model systems. The underlying mechanisms by which AntiOxCIN$_3$ and other mitochondriotropic antioxidants influence mitochondrial membrane structure is currently being studied by our group and will be object of a follow up study.

In conclusion, herein we provide an innovative toolbox of biophysical studies, in silico predictors and lipid nanosystems used as mimetic models to study the interaction between the drug and biological interfaces towards a comprehensive molecular-level understanding of drug's biodistribution profile. This toolbox is a simple and useful approach for predicting future pharmacokinetic issues of novel drug candidates, in the early stages of pre-clinical studies of the drug development process. It can be used to scrutinize several optimize leads and select the ones that have potential better biodistribution profile to be tested in vivo. These in vitro assays are not surrogating in vivo assays, as they have limitations in mimicking the complexity of biological barriers but will be essential to understand the molecular-level properties of novel drugs and drug candidates. Moreover, under controlled conditions that are not feasible in vivo, the in vitro assays may help to rationalize and predict interactions with the bioenvironment. Finally, the work herein proposed is a contribution for the protection of animals used for scientific purposes (Directive 2010/63/EU) in agreement with the EU principles of Replacement (of animals for other in vitro models), Reduction (of animal tests) and Refinement (the "Three Rs").

Acknowledgments

This work was supported by Fundação para a Ciência e Tecnologia (FCT) in the framework of the Strategic Funding Funding [UID/FIS/04650/2019], and by the project CONCERT [POCI-01-0145-FEDER-032651 and PTDC/NAN-MAT/326512017], co-financed by the European Regional Development Fund (ERDF), through COMPETE 2020, under Portugal 2020, and FCT I.P. The authors thank Elettra Sincrotone, Trieste, Italy, for beam time and support through the project 20155321. We also acknowledge UIDB/00081/2020, PTDC/MED-FAR/29391/2017, PTDC/BIA-MOL/28607/2017, PTDC/MED-QUI/29164/2017. M Lúcio thanks FCT and ERDF for doctoral position [CTTI-150/18-CF (1)] in the ambit of the project CONCERT. Jana Nieder acknowledges funding by the CCDR-N via the grant: NORTE-01-0145-FEDER-000019. Sofia Benfeito and Eduarda Fernandes (SFRH/BD/147938/2019) grants are supported by FCT, POPH and FEDER/COMPETE.

Disclosure

The authors report no conflicts of interest in this work.

References

1. Finkel T, Holbrook NJ. Oxidants, oxidative stress and the biology of ageing. *Nature*. 2000;408(6809):239–247. doi:10.1038/35041687
2. Islam MT. Oxidative stress and mitochondrial dysfunction-linked neurodegenerative disorders. *Neurol Res*. 2017;39(1):73–82. doi:10.1080/01616412.2016.1251711
3. Scandalios JG. Genomic responses to oxidative stress. *Mol Cell Biol Mol Med*. 2006;489–512.
4. Cooke MS, Evans MD, Dizdaroglu M, Lunec J. Oxidative DNA damage: mechanisms, mutation, and disease. *FASEB J*. 2003;17(10):1195–1214. doi:10.1096/fj.02-0752rev
5. Chakravarti B, Chakravarti DN. Oxidative modification of proteins: age-related changes. *Gerontology*. 2007;53(3):128–139. doi:10.1159/000097865
6. Ballatore C, Huryn DM, Smith AB 3rd. Carboxylic acid (bio)isosteres in drug design. *ChemMedChem*. 2013;8(3):385–395. doi:10.1002/cmdc.201200585
7. Murphy MP. Targeting lipophilic cations to mitochondria. *Biochim Biophys Acta*. 2008;1777(7–8):1028–1031. doi:10.1016/j.bbabio.2008.03.029
8. Smith RA, Murphy MP. Mitochondria-targeted antioxidants as therapies. *Discov Med*. 2011;11(57):106–114.
9. Amorim R, Benfeito S, Teixeira J, Cagide F, Oliveira PJ, Borges F. Targeting mitochondria: the road to mitochondriotropic antioxidants and beyond. *Mitochondrial Biol Exp Ther*. 2018;333–358.
10. Teixeira J, Cagide F, Benfeito S, et al. Development of a mitochondriotropic antioxidant based on caffeic acid: proof of concept on cellular and mitochondrial oxidative stress models. *J Med Chem*. 2017;60(16):7084–7098. doi:10.1021/acs.jmedchem.7b00741
11. Lipinski CA, Lombardo F, Dominy BW, Feeney PJ. Experimental and computational approaches to estimate solubility and permeability in drug discovery and development settings. *Adv Drug Deliv Rev*. 2001;46(1–3):3–26. doi:10.1016/S0169-409X(00)00129-0
12. Benfeito S, Oliveira C, Fernandes C, et al. Fine-tuning the neuroprotective and blood-brain barrier permeability profile of multi-target agents designed to prevent progressive mitochondrial dysfunction. *Eur J Med Chem*. 2019;167:525–545. doi:10.1016/j.ejmech.2019.01.055
13. Murphy MP, Smith RA. Targeting antioxidants to mitochondria by conjugation to lipophilic cations. *Annu Rev Pharmacol Toxicol*. 2007;47(1):629–656. doi:10.1146/annurev.pharmtox.47.120505.105110
14. Teixeira J, Oliveira C, Amorim R, et al. Development of hydroxybenzoic-based platforms as a solution to deliver dietary antioxidants to mitochondria. *Sci Rep*. 2017;7(1):6842. doi:10.1038/s41598-017-07272-y

15. Liu X, Testa B, Fahr A. Lipophilicity and its relationship with passive drug permeation. *Pharm Res*. 2011;28(5):962–977. doi:10.1007/s11095-010-0303-7
16. Di L, Kerns EH. *Drug-Like Properties: Concepts, Structure Design and Methods from ADME to Toxicity Optimization*. Elsevier Science; 2015.
17. Seydel JK. Drug-membrane interaction and pharmacokinetics of drugs. *Drug Membrane Interact*. 2003;141–215.
18. Pignatello R, Musumeci T, Basile L, Carbone C, Puglisi G. Biomembrane models and drug-biomembrane interaction studies: involvement in drug design and development. *J Pharm Bioallied Sci*. 2011;3(1):4–14. doi:10.4103/0975-7406.76461
19. Lucio M, Lima JL, Reis S. Drug-membrane interactions: significance for medicinal chemistry. *Curr Med Chem*. 2010;17(17):1795–1809. doi:10.2174/092986710791111233
20. Stefaniu C, Brezesinski G, Mohwald H. Langmuir monolayers as models to study processes at membrane surfaces. *Adv Colloid Interface Sci*. 2014;208:197–213. doi:10.1016/j.cis.2014.02.013
21. Fernandes E, Soares TB, Goncalves H, et al. A molecular biophysical approach to diclofenac topical gastrointestinal damage. *Int J Mol Sci*. 2018;19(11):3411. doi:10.3390/ijms19113411
22. Lúcio M, Bringezu F, Reis S, Lima JLFC, Brezesinski G. Binding of nonsteroidal anti-inflammatory drugs to DPPC: structure and thermodynamic aspects. *Langmuir*. 2008;24(8):4132–4139. doi:10.1021/la703584s
23. Lucio M, Ferreira H, Lima FC, Reis S. Interactions between oxicams and membrane bilayers: an explanation for their different COX selectivity. *Med Chem (Los Angeles)*. 2006;2(5):447–456. doi:10.2174/157340606778250199
24. Lúcio M, Ferreira H, Lima JLFC, Reis S. Use of liposomes as membrane models to evaluate the contribution of drug–membrane interactions to antioxidant properties of etodolac. *Redox Rep*. 2013;13(5):225–236. doi:10.1179/135100008X308939
25. Lúcio M, Ferreira H, Lima JLFC, Reis S. Use of liposomes to evaluate the role of membrane interactions on antioxidant activity. *Anal Chim Acta*. 2007;597(1):163–170. doi:10.1016/j.aca.2007.06.039
26. Nunes C, Brezesinski G, Lima JL, Reis S, Lucio M. Synchrotron SAXS and WAXS study of the interactions of NSAIDs with lipid membranes. *J Phys Chem B*. 2011;115(24):8024–8032. doi:10.1021/jp2025158
27. Nunes C, Brezesinski G, Pereira-Leite C, Lima JL, Reis S, Lucio M. NSAIDs interactions with membranes: a biophysical approach. *Langmuir*. 2011;27(17):10847–10858. doi:10.1021/la201600y
28. Nunes C, Brezesinski G, Lopes D, Lima JLFC, Reis S, Lúcio M. Lipid–drug interaction: biophysical effects of tolmetin on membrane mimetic systems of different dimensionality. *J Phys Chem B*. 2011;115(43):12615–12623. doi:10.1021/jp206013z
29. Bailey-Hytholt CM, Shen TL, Nie B, Tripathi A, Shukla A. Placental trophoblast-inspired lipid bilayers for cell-free investigation of molecular interactions. *ACS Appl Mater Interfaces*. 2020;12(28):31099–31111. doi:10.1021/acsami.0c06197
30. Uehara TM, Marangoni VS, Pasquale N, Miranda PB, Lee KB, Zucolotto V. A detailed investigation on the interactions between magnetic nanoparticles and cell membrane models. *ACS Appl Mater Interfaces*. 2013;5(24):13063–13068. doi:10.1021/am404042r
31. Khadka Nawal K, Cheng X, Ho Chian S, Katsaras J, Pan J. Interactions of the anticancer drug tamoxifen with lipid membranes. *Biophys J*. 2015;108(10):2492–2501. doi:10.1016/j.bpj.2015.04.010
32. Sarpietro MG, Accolla ML, Santoro N, et al. Calorimetry and Langmuir–Blodgett studies on the interaction of a lipophilic prodrug of LHRH with biomembrane models. *J Colloid Interface Sci*. 2014;421:122–131. doi:10.1016/j.jcis.2014.01.040
33. Peetla C, Stine A, Labhasetwar V. Biophysical interactions with model lipid membranes: applications in drug discovery and drug delivery. *Mol Pharm*. 2009;6(5):1264–1276. doi:10.1021/mp9000662
34. Fernandes E, Soares TB, Goncalves H, Lucio M. Spectroscopic studies as a toolbox for biophysical and chemical characterization of lipid-based nanotherapeutics. *Front Chem*. 2018;6:323. doi:10.3389/fchem.2018.00323
35. Seddon AM, Casey D, Law RV, Gee A, Templer RH, Ces O. Drug interactions with lipid membranes. *Chem Soc Rev*. 2009;38(9):2509. doi:10.1039/b813853m
36. Bunea A-I, Harloff-Helleberg S, Taboryski R, Nielsen HM. Membrane interactions in drug delivery: model cell membranes and orthogonal techniques. *Adv Colloid Interface Sci*. 2020;281:281. doi:10.1016/j.cis.2020.102177
37. Jelinek R, Kolusheva S. Membrane interactions of host-defense peptides studied in model systems. *Curr Protein Pept Sci*. 2005;6(1):103–114. doi:10.2174/1389203053027511
38. Nunes C, Sousa CT, Proença MP, et al. Synchrotron small angle X-ray scattering for the evaluation of the interaction of silica nanotubes with lipid membranes. *RSC Adv*. 2013;3(26):10323. doi:10.1039/c3ra22974b
39. Wang S, Guo H, Li Y, Li X. Penetration of nanoparticles across a lipid bilayer: effects of particle stiffness and surface hydrophobicity. *Nanoscale*. 2019;11(9):4025–4034. doi:10.1039/C8NR09381D
40. Monteiro JP, Martins AF, Lucio M, et al. Nimesulide interaction with membrane model systems: are membrane physical effects involved in nimesulide mitochondrial toxicity? *Toxicol in Vitro*. 2011;25(6):1215–1223. doi:10.1016/j.tiv.2011.05.014
41. Hu X, Tam K. Biomembrane mimics and their roles in anti-bacterial drug discovery. *ADMET DMPK*. 2017;5(1):9. doi:10.5599/admet.5.1.375
42. Sarkis J, Vie V. Biomimetic models to investigate membrane biophysics affecting lipid-protein interaction. *Front Bioeng Biotechnol*. 2020;8:270. doi:10.3389/fbioe.2020.00270
43. Jojart B, Posa M, Fiser B, Szori M, Farkas Z, Viskolcz B. Mixed micelles of sodium cholate and sodium dodecylsulphate 1:1 binary mixture at different temperatures–experimental and theoretical investigations. *PLoS One*. 2014;9(7):e102114. doi:10.1371/journal.pone.0102114
44. Magalhaes LM, Nunes C, Lucio M, Segundo MA, Reis S, Lima JL. High-throughput microplate assay for the determination of drug partition coefficients. *Nat Protoc*. 2010;5(11):1823–1830. doi:10.1038/nprot.2010.137
45. Lakowicz JR. *Principles of Fluorescence Spectroscopy*. 3 ed. Springer US; 2006.
46. Musteata FM. Clinical utility of free drug monitoring. *Ther Drug Monit*. 2012;75–101.
47. Rahnama E, Mahmoodian-Moghaddam M, Khorsand-Ahmadi S, Saberi MR, Chamani J. Binding site identification of metformin to human serum albumin and glycated human serum albumin by spectroscopic and molecular modeling techniques: a comparison study. *J Biomol Struct Dyn*. 2015;33(3):513–533. doi:10.1080/07391102.2014.893540
48. Carvalho AM, Fernandes E, Goncalves H, et al. Prediction of paclitaxel pharmacokinetic based on in vitro studies: interaction with membrane models and human serum albumin. *Int J Pharm*. 2020;580:119222. doi:10.1016/j.ijpharm.2020.119222
49. Seydel JK, Wiese M. *Drug-Membrane Interactions Analysis, Drug Distribution, Modeling*. Vol. 5. Weinheim: Wiley-VCH; 2002.
50. van de Waterbeemd H, Kansy M. Hydrogen-bonding capacity and brain penetration. *CHIMIA Int J Chem*. 1992;46(7–8):299–303.
51. Liu X, Tu M, Kelly RS, Chen C, Smith BJ. Development of a computational approach to predict blood-brain barrier permeability. *Drug Metab Dispos*. 2004;32(1):132–139. doi:10.1124/dmd.32.1.132
52. Korzekwa K, Nagar S. Drug distribution part 2. predicting volume of distribution from plasma protein binding and membrane partitioning. *Pharm Res*. 2017;34(3):544–551. doi:10.1007/s11095-016-2086-y
53. Lombardo F, Obach RS, Shalaeva MY, Gao F. Prediction of volume of distribution values in humans for neutral and basic drugs using physicochemical measurements and plasma protein binding data. *J Med Chem*. 2002;45(13):2867–2876. doi:10.1021/jm0200409

54. Waters LJ, Shokry DS, Parkes GM. Predicting human intestinal absorption in the presence of bile salt with micellar liquid chromatography. *Biomed Chromatogr*. 2016;30(10):1618–1624. doi:10.1002/bmc.3731
55. Clark DE. Rapid calculation of polar molecular surface area and its application to the prediction of transport phenomena. 1. Prediction of intestinal absorption. *J Pharm Sci*. 1999;88(8):807–814. doi:10.1021/js9804011
56. Kramer SD. Absorption prediction from physicochemical parameters. *Pharm Sci Technolo Today*. 1999;2(9):373–380. doi:10.1016/S1461-5347(99)00188-1
57. Camenisch G, Alsenz J, Waterbeemd Hvd FG, Folkers G. Estimation of permeability by passive diffusion through Caco-2 cell monolayers using the drugs' lipophilicity and molecular weight. *Eur J Pharm Sci*. 1998;6(4):313–319. doi:10.1016/S0928-0987(97)10019-7
58. Katayama K, Fujita T. Studies on lymphatic absorption of 1′,2′-(3 H)-coenzyme Q 10 in rats. *Chem Pharm Bull (Tokyo)*. 1972;20(12):2585–2592. doi:10.1248/cpb.20.2585
59. Zaki NM. Strategies for oral delivery and mitochondrial targeting of CoQ10. *Drug Deliv*. 2016;23(6):1868–1881. doi:10.3109/10717544.2014.993747
60. Lambrinidis G, Vallianatou T, Tsantili-Kakoulidou A. In vitro, in silico and integrated strategies for the estimation of plasma protein binding. A review. *Adv Drug Deliv Rev*. 2015;86:27–45.
61. Wan H, Holmen A. High throughput screening of physicochemical properties and in vitro ADME profiling in drug discovery. *Comb Chem High Throughput Screen*. 2009;12(3):315–329. doi:10.2174/138620709787581701
62. Naik KM, Kolli DB, Nandibewoor ST. Elucidation of binding mechanism of hydroxyurea on serum albumins by different spectroscopic studies. *Springerplus*. 2014;3(1):360. doi:10.1186/2193-1801-3-360
63. Shamsi A, Ahmed A, Bano B. Probing the interaction of anticancer drug temsirolimus with human serum albumin: molecular docking and spectroscopic insight. *J Biomol Struct Dyn*. 2018;36(6):1479–1489. doi:10.1080/07391102.2017.1326320
64. Shamsi A, Ahmed A, Khan MS, Husain FM, Bano B. Rosmarinic acid restrains protein glycation and aggregation in human serum albumin: multi spectroscopic and microscopic insight - possible therapeutics targeting diseases. *Int J Biol Macromol*. 2020;161(161):187–193. doi:10.1016/j.ijbiomac.2020.06.048
65. Shamsi A, Ahmed A, Khan MS, Al Shahwan M, Husain FM, Bano B. Understanding the binding between rosmarinic acid and serum albumin: in vitro and in silico insight. *J Mol Liq*. 2020;311(311):113348. doi:10.1016/j.molliq.2020.113348
66. Precupas A, Sandu R, Leonties AR, Anghel D-F, Popa VT. Complex interaction of caffeic acid with bovine serum albumin: calorimetric, spectroscopic and molecular docking evidence. *New J Chem*. 2017;41(24):15003–15015. doi:10.1039/C7NJ03410E
67. Hu YJ, Li W, Liu Y, Dong JX, Qu SS. Fluorometric investigation of the interaction between methylene blue and human serum albumin. *J Pharm Biomed Anal*. 2005;39(3–4):740–745. doi:10.1016/j.jpba.2005.04.009
68. Anwar S, Shamsi A, Kar RK, et al. Structural and biochemical investigation of MARK4 inhibitory potential of cholic acid: towards therapeutic implications in neurodegenerative diseases. *Int J Biol Macromol*. 2020;161:596–604. doi:10.1016/j.ijbiomac.2020.06.078
69. Anwar S, Shamsi A, Shahbaaz M, et al. Rosmarinic acid exhibits anticancer effects via MARK4 inhibition. *Sci Rep*. 2020;10(1). doi:10.1038/s41598-020-65648-z.
70. Ross PD, Subramanian S. Thermodynamics of protein association reactions: forces contributing to stability. *Biochemistry*. 1981;20(11):3096–3102. doi:10.1021/bi00514a017
71. Satish L, Rana S, Arakha M, et al. Impact of imidazolium-based ionic liquids on the structure and stability of lysozyme. *Spectrosc Lett*. 2016;49(6):383–390. doi:10.1080/00387010.2016.1167089
72. Suvarna M, Dyawanapelly S, Kansara B, Dandekar P, Jain R. Understanding the stability of nanoparticle–protein interactions: effect of particle size on adsorption, conformation and thermodynamic properties of serum albumin proteins. *ACS Appl Nano Mater*. 2018;1(10):5524–5535. doi:10.1021/acsanm.8b01019
73. Yamasaki K, Chuang VT, Maruyama T, Otagiri M. Albumin-drug interaction and its clinical implication. *Biochim Biophys Acta*. 2013;1830(12):5435–5443. doi:10.1016/j.bbagen.2013.05.005
74. Li Y, Fawcett JP, Zhang H, Tucker IG. Transport and metabolism of MitoQ10, a mitochondria-targeted antioxidant, in Caco-2 cell monolayers. *J Pharm Pharmacol*. 2007;59(4):503–511. doi:10.1211/jpp.59.4.0004
75. Bemporad D, Essex JW, Luttmann C. Permeation of small molecules through a lipid bilayer: a computer simulation study. *J Phys Chem B*. 2004;108(15):4875–4884. doi:10.1021/jp035260s
76. van Balen GP, Martinet C, Caron G, et al. Liposome/water lipophilicity: methods, information content, and pharmaceutical applications. *Med Res Rev*. 2004;24(3):299–324. doi:10.1002/med.10063
77. Di L, Kerns EH. Profiling drug-like properties in discovery research. *Curr Opin Chem Biol*. 2003;7(3):402–408. doi:10.1016/S1367-5931(03)00055-3
78. Ballard P, Brassil P, Bui KH, et al. Metabolism and pharmacokinetic optimization strategies in drug discovery. *Drug Des Devel*. 2013;135–155.
79. Greenblatt DJ, Abernethy DR, Divoll M. Is volume of distribution at steady state a meaningful kinetic variable? *J Clin Pharmacol*. 1983;23(8–9):391–400. doi:10.1002/j.1552-4604.1983.tb02753.x
80. Filler G. Extracorporeal therapies for poisoning. *Compr Pediatr Nephrol*. 2008;1045–1052.
81. Saha S, Panieri E, Suzen S, Saso L. The interaction of flavonols with membrane components: potential effect on antioxidant activity. *J Membr Biol*. 2020;253(1):57–71. doi:10.1007/s00232-019-00105-1
82. Simons K, Vaz WL. Model systems, lipid rafts, and cell membranes. *Annu Rev Biophys Biomol Struct*. 2004;33(1):269–295. doi:10.1146/annurev.biophys.32.110601.141803
83. Poojari C, Wilkosz N, Lira RB, et al. Behavior of the DPH fluorescence probe in membranes perturbed by drugs. *Chem Phys Lipids*. 2019;223:104784. doi:10.1016/j.chemphyslip.2019.104784
84. Marsh D, Watts A, Knowles PF. Cooperativity of the phase transition in single- and multibilayer lipid vesicles. *Biochim Biophys Acta Biomembr*. 1977;465(3):500–514. doi:10.1016/0005-2736(77)9028-1
85. Michel N, Fabiano AS, Polidori A, Jack R, Pucci B. Determination of phase transition temperatures of lipids by light scattering. *Chem Phys Lipids*. 2006;139(1):11–19. doi:10.1016/j.chemphyslip.2005.09.003
86. Domínguez A, Álvarez A, Hilario E, Suarez-Merino B, Goñi-de-Cerio F. Central nervous system diseases and the role of the blood-brain barrier in their treatment. *Neurosci Discov*. 2013;1(1):3. doi:10.7243/2052-6946-1-3
87. Carpenter TS, Kirshner DA, Lau EY, Wong SE, Nilmeier JP, Lightstone FC. A method to predict blood-brain barrier permeability of drug-like compounds using molecular dynamics simulations. *Biophys J*. 2014;107(3):630–641. doi:10.1016/j.bpj.2014.06.024
88. Oliveira C, Bagetta D, Cagide F, et al. Benzoic acid-derived nitrones: a new class of potential acetylcholinesterase inhibitors and neuroprotective agents. *Eur J Med Chem*. 2019;174:116–129. doi:10.1016/j.ejmech.2019.04.026
89. Koynova R, Macdonald RC. Natural lipid extracts and biomembrane-mimicking lipid compositions are disposed to form nonlamellar phases, and they release DNA from lipoplexes most efficiently. *Biochim Biophys Acta*. 2007;1768(10):2373–2382. doi:10.1016/j.bbamem.2007.04.026
90. Ibarguren M, Lopez DJ, Escriba PV. The effect of natural and synthetic fatty acids on membrane structure, microdomain organization, cellular functions and human health. *Biochim Biophys Acta*. 2014;1838(6):1518–1528. doi:10.1016/j.bbamem.2013.12.021

91. Lopez S, Bermudez B. Membrane composition and dynamics: a target of bioactive virgin olive oil constituents. *Biochim Biophys Acta*. 2014;1838(6):1638–1656.
92. Hoekstra D, Martin OC. Transbilayer redistribution of phosphatidylethanolamine during fusion of phospholipid vesicles. Dependence on fusion rate, lipid phase separation, and formation of nonbilayer structures. *Biochemistry*. 1982;21(24):6097–6103. doi:10.1021/bi00267a011
93. Rappolt M, Hickel A, Bringezu F, Lohner K. Mechanism of the lamellar/inverse hexagonal phase transition examined by high resolution x-ray diffraction. *Biophys J*. 2003;84(5):3111–3122. doi:10.1016/S0006-3495(03)70036-8
94. Corazzi L, Roberti R. Lipids of brain mitochondria. *Handbook Neurochem Mol Neurobiol*. 2009;199–221.
95. Carvalho C, Moreira PI. Oxidative stress: a major player in cerebrovascular alterations associated to neurodegenerative events. *Front Physiol*. 2018;9:806. doi:10.3389/fphys.2018.00806